Drug Resistance Updates 85 (2026) 101354

Contents lists available at ScienceDirect

Drug Resistance Updates

journal homepage: www.elsevier.com/locate/drup

Single-cell transcriptome analysis of patient-derived organoids captures inter- and intratumor heterogeneity and uncovers targetable pathways in high grade serous ovarian cancer

Marco Pieraccioli [a,b,1], Alessandra Ciucci [a,b,1], Christian Corti [b], Roberta Mastrantonio [c], Eleonora Kristina Scarpone [b], Eleonora Cesari [b], Alessia Piermattei [d], Angelo Minucci [e,f], Andrea Urbani [f,g], Floriana Camarda [c,h], Anna Fagotti [c,h], Luca Tamagnone [c,i], Giovanni Scambia [c,h], Camilla Nero [c,h,*], Claudio Sette [a,b,**]

[a] Department of Neuroscience, Section of Human Anatomy, Catholic University of the Sacred Heart, Rome 00168, Italy
[b] GSTeP Organoids Research Core Facility, IRCCS Fondazione Policlinico A. Gemelli, Rome 00168, Italy
[c] Department of Life Sciences and Public Health, Catholic University of the Sacred Heart, Rome 00168, Italy
[d] Gynecopathology and Breast Pathology Unit, Department of Women, Children and Public Health Sciences, Fondazione Policlinico A. Gemelli IRCCS, Rome 00168, Italy
[e] Departmental Unit of Molecular and Genomic Diagnostics, GSTeP Genomics Core Facility, Fondazione Policlinico A. Gemelli IRCCS, Rome 00168, Italy
[f] Clinical Chemistry, Biochemistry and Molecular Biology Operations (UOC), Fondazione Policlinico A. Gemelli IRCCS, Rome 00168, Italy
[g] Department of Basic Biotechnological Sciences, Intensive Care and Perioperative Clinics Research, Catholic University of the Sacred Heart, Università Cattolica del Sacro Cuore, Rome 00168, Italy
[h] Unit of Oncological Gynecology, Department of Women, Children and Public Health Sciences, Fondazione Policlinico A. Gemelli IRCCS, Rome 00168, Italy
[i] GSTeP Liquid Biopsy Core Facility, IRCCS Fondazione Policlinico A. Gemelli, Rome 00168, Italy

ARTICLE INFO

Keywords:
High grade serous ovarian cancer
Patient-derived organoids
Platinum resistance
Oxidative phosphorylation
Major histocompatibility complex type II

ABSTRACT

Aim: High grade serous ovarian cancer (HGSOC) is the most aggressive subtype of ovarian cancer. HGSOC is characterized by high inter- and intra-tumoral heterogeneity, which contributes to chemotherapy resistance. Patient-derived organoids (PDOs) are valuable preclinical models to elucidate the biology of human cancers and to test their response to treatments. This study aims at characterizing the cellular heterogeneity of PDOs and to uncover vulnerabilities of chemotherapy resistant HGSOC.

Methods: Single-cell transcriptomics of PDOs developed from biopsies of platinum-resistant and platinum-sensitive HGSOC. Chemotherapeutic treatments of HGSOC PDOs and of ascitic-derived ovarian cancer cells and immunohistochemistry analyses of tissues from independent HGSOC patients.

Results: HGSOC PDOs comprise subclusters of cells exhibiting different transcriptional states and patient-specific signatures. Proliferative and non-proliferative subclusters co-exist in PDOs and their relative proportion is altered by chemotherapy. Proliferative cell sub-populations exhibit expression of cell cycle and DNA damage response related genes, whereas non-proliferative sub-populations display inflammatory signatures. Furthermore, sensitivity to platinum-based treatments was inversely correlated with oxidative phosphorylation (OXHPOS) in PDOs, indicating a metabolic switch associated with chemoresistance. Accordingly, platinum-resistant PDOs and ascitic HGSOC cells show higher sensitivity to OXHPOS inhibition. We found that neoadjuvant chemotherapy (NACT) directly up-regulates oncogenic and metabolic pathways that are involved in development of recurrence, such as the *MYC* and OXPHOS genes. NACT also induces the expression of major histocompatibility complex type II (MHC-II) molecules. Immunohistochemistry confirmed MHC-II up-regulation in post-NACT biopsies, indicating that tumour cells mount a general antigen-presenting response upon chemotherapy, associated with recruitment of infiltrating immune cells.

* Corresponding author at: Unit of Oncological Gynecology, Department of Women, Children and Public Health Sciences, Fondazione Policlinico A. Gemelli IRCCS, Rome 00168, Italy.
** Corresponding author at: Department of Neuroscience, Section of Human Anatomy, Catholic University of the Sacred Heart, Rome 00168, Italy.
E-mail addresses: camilla.nero@policlinicogemelli.it (C. Nero), claudio.sette@unicatt.it (C. Sette).
[1] These authors equally contributed to this study

https://doi.org/10.1016/j.drup.2026.101354
Received 8 September 2025; Received in revised form 23 December 2025; Accepted 6 January 2026
Available online 8 January 2026

Conclusion: PDOs maintain the inter- and intra-tumoral cellular heterogeneity of HGSOC. Chemotherapy targets proliferative cell subclusters, sparing non-proliferative ones. Dependency on OXPHOS represents an actionable vulnerability in PDOs, which can be exploited to hijack chemoresistance. Sequential chemotherapy and immunotherapy may also improve clinical response of HGSOC patients.

Introduction

High grade serous ovarian cancer (HGSOC) is the most lethal form of ovarian cancer, accounting for 70 % of diagnosed cases (Vaughan et al., 2011; Veneziani et al., 2023). Presentation of disease at advanced and metastatic stages contributes to its poor prognosis. Complete cytoreductive surgery, followed by platinum-based chemotherapy and maintenance therapy with inhibitors of poly (ADP-ribose) polymerase (PARPi) and/or vascular endothelial growth factor (VEGFi), represents the most curative treatment for HGSOC patients. Nevertheless, most tumors relapse with aggressive phenotypes, leading to a 5-year survival rate < 50 % (Lheureux et al., 2019b; Vaughan et al., 2011). In this dismal scenario, the identification of molecular aberrations driving the onset and progression of HGSOC in the last decades has revolutionized the clinical approach to this cancer. HGSOC is characterized by almost ubiquitous mutations in the *TP53* gene, high genome instability (GI) and frequent homologous recombination deficiency (HRD). A HRD phenotype is observed in ~50 % of HGSOC patients and arises from mutations in genes encoding for proteins involved in DNA repair by HR, such as *BRCA1* and *BRCA2*, and/or in the DNA damage response (DDR) pathway (Cancer Genome Atlas Research, 2011; Veneziani et al., 2023). Together with *TP53* inactivation, mutations in HR/DDR genes confer high sensitivity of HGSOC to DNA damaging agents or to drugs that interfere with DNA repair mechanisms, such as the PARPi (Vergote et al., 2022b). Coherently, presence of HRD-associated mutations predicts improved prognosis in HGSOC (Macintyre et al., 2018; Norquist et al., 2018). *CCNE1* amplification is another frequent genomic alteration in HGSOC, detected in ~20 % of patients. Deregulated expression of cyclin E1 leads to unscheduled DNA replication and GI, while conferring reduced sensitivity to DNA-damaging agents (Gorski et al., 2020) and an immunologically inert phenotype (Vazquez-Garcia et al., 2022). Notably, *BRCA1* mutations and *CCNE1* amplification are mutually exclusive, as their concomitant alteration causes synthetic lethality (Etemadmoghadam et al., 2013). However, while these genetic hallmarks are clinically relevant and guide treatment decisions, most HGSOC cases present with intra-patient genetic and phenotypic heterogeneity (Lheureux et al., 2019a; Lheureux et al., 2019b; Veneziani et al., 2023), which is likely due to the early functional inactivation of *TP53* and the consequent GI-driven progressive evolutionary divergence (Macintyre et al., 2018). Genetic heterogeneity contributes to the selection or evolution of chemoresistant clones during therapy and to disease recurrence.

Single-cell transcriptome analysis of HGSOC primary lesions, ascites and metastases from multiple anatomical sites has revealed the existence of clusters of tumor cells enriched for specific biological processes, including inflammatory, TGFβ and hypoxia signalling pathways (Vazquez-Garcia et al., 2022). Clusters enriched in immune system response signatures were specifically increased in HRD tumors. Moreover, these clusters also featured the up-regulation of major histocompatibility complex (MHC) I and II genes and were associated with a specific immune infiltrate phenotype (Vazquez-Garcia et al., 2022). While intra-patient heterogeneity is likely associated to the mutational status of tumor cells (McPherson et al., 2025), other studies also indicated the existence of non-genetic drivers of phenotypic diversity in HGSOC cells (Hu et al., 2020). Together, these findings suggest that elucidation of tumor cell subtypes may reveal specific features of co-existing HGSOC cells and uncover new targetable vulnerabilities for this cancer.

Patient-derived organoids (PDOs) have emerged as powerful preclinical models that capture the genomic and phenotypic features of tumors (Kim et al., 2025), including HGSOC (Lohmussaar et al., 2020; Nero et al., 2021). PDOs recapitulate the response of the original tumors to therapeutic treatments, thus representing valuable avatars for testing new treatments (Kim et al., 2025). Herein, we have characterized HGSOC PDOs from tumor biopsies of patients who resulted sensitive or resistant to platinum-based chemotherapy, including two lines derived from biopsies taken before and after neoadjuvant chemotherapy (NACT) of the same patient. Our data indicate that HGSOC PDOs maintain the cellular heterogeneity that characterizes tumor cell subclusters *in vivo*. We also provide evidence that platinum-based chemotherapy represents a driving force for the selection of specific transcriptional states in HGSOC cells, including up-regulation of MHC-II molecules. Lastly, we found that platinum-resistant HGSOC cells are characterized by an oxidative phosphorylation (OXPHOS) signature, and that this metabolic dependency can be exploited to selectively kill chemoresistant cells.

Results

HGSOC PDOs comprise cells with distinct transcriptional states

Intratumoral heterogeneity is a hallmark of HGSOC, which impacts on the response to therapies and disease recurrence in patients (Veneziani et al., 2023). To investigate whether heterogeneity in transcriptional states also characterizes HGSOC PDOs, we selected samples from eight patients who exhibited different responses to platinum-based chemotherapy (Fig. 1A, Table S1). Five of these patients (HGSOC-33, HGSOC-85, HGSOC-108, HGSOC-117 and HGSOC-121) positively responded to chemotherapy (recurrence after $\geq$10 months), whereas three of them (HGSOC-24, HGSOC-36 and HGSOC-122) recurred within 6 months and were clinically classified as platinum-resistant (Table S1). PDO lines were developed from either diagnostic laparoscopic biopsies (LPS) or primary debulking surgery (PDS) biopsy (Table S1). For patient HGSOC-33, who underwent interval debulking surgery (IDS) after the first three cycles of platinum-based NACT, we were also able to develop a PDO line (PDO-33.2) from the IDS (Table S1), thus allowing analysis of tumor evolution during chemotherapy. Genomic analyses showed that the post-NACT PDO-33.2 maintained all mutations present in the pre-NACT PDO-33.3 and its corresponding parental tumor tissue, except for a non-synonymous mutation in the *PIK3R3* gene. In addition, PDO-33.2 also featured *de novo* mutations in the *FGF6*, *FGF23*, *FGFR1*, *MDM2* and *ZNF703* genes (Fig. S1A). Morphological analysis of the established PDO lines showed the irregular shape and variable morphology (Fig. S1B,C) that was previously reported for HGSOC PDOs (Kopper et al., 2019). Sensitivity to carboplatin of the nine PDO lines ranged from 2.8 μM to 45 μM (Fig. 1D), thus featuring the heterogeneous response observed in HGSOC treatment. Interestingly, the post-NACT PDO-33.2 displayed a slightly higher (~1.3-fold) IC_{50} than PDO-33.3 established from the chemotherapy naïve biopsy of the same patient (Fig. 1D).

To explore the cellular heterogeneity of HGSOC PDOs and its potential role in driving chemotherapeutic resistance, we carried out whole transcriptome single-cell RNA sequencing (scRNA-seq) analyses from the nine PDO lines (Fig. S1D). After standard quality filtering (see Methods), a total of 29735 single cells were retained for analysis (Fig. 1E). Unsupervised graph-based clustering and visualization via t-distributed Stochastic Neighbor Embedding (t-SNE) analyses showed that most cells from each PDO clustered together, indicating patient-specific transcriptional signatures (Fig. 1E). As expected for epithelial-

derived PDOs, gene expression profiles confirmed the epithelial identity of all cells (Fig. S1E). Expression of epithelial cancer cell markers (*EPCAM*, *KRT8*, *KRT18*) and of well-established positive (*PAX8*, *WT1*, *MUC16*) and negative (*KRT20*) diagnostic markers for HGSOC confirmed that all cells belong to malignant epithelial cells (Fig. S1F). Furthermore, except for PDO-117.3, we identified intra-patient heterogeneity in HGSOC PDOs, with each line comprising either two or three separate clusters (Fig. 1F). Identification of the top 10 genes that mostly characterized each cluster showed high similarities in gene expression between clusters of the same PDO, which were clearly separated from those of the other PDOs (Fig. S2A,B; Table S2A). These observations indicate that PDOs in culture retain the inter-tumoral and intra-tumoral cellular heterogeneity of HGSOC, suggesting that analyses of PDO clusters may reveal transcriptional states that characterize the complex phenotype of this cancer.

Proliferative and non-proliferative cells co-exist in cultured HGSOC PDOs

Computational analyses of cluster-associated gene expression signatures highlighted the cancer hallmarks that are featured by each cell cluster of the nine HGSOC PDOs (Fig. 2A). Interestingly, hallmarks of cell proliferation, such as G2/M checkpoint, E2F targets and mitotic spindle, were selectively enriched only in one or two (PDO-108.3) of the clusters of each PDO line (Fig. 2A). This observation suggests the co-existence of proliferative (clusters 3, 4, 7, 8, 12, 15, 16, 18, 19) and non-proliferative (clusters 0, 1, 2, 5, 6, 9, 10, 11, 13, 14, 17) subpopulations of cells in each PDO. Coherently, "proliferative" clusters exhibit a highly significant enrichment in mitotic hallmarks (Fig. 2B, Fig. S3A) and express markers of the G1-S transition (*E2F1*), S (*CCNE2*) and G2-M phases (*CCNA2* and *CCNB1*) of the cell cycle (Fig. 2C,D and Fig. S3B). T-SNE clustering of these mitotic genes clearly separated the proliferative and non-proliferative cells in each PDO and allowed visualization of cells in different phases of the cell cycle within the proliferative clusters (Fig. 2E).

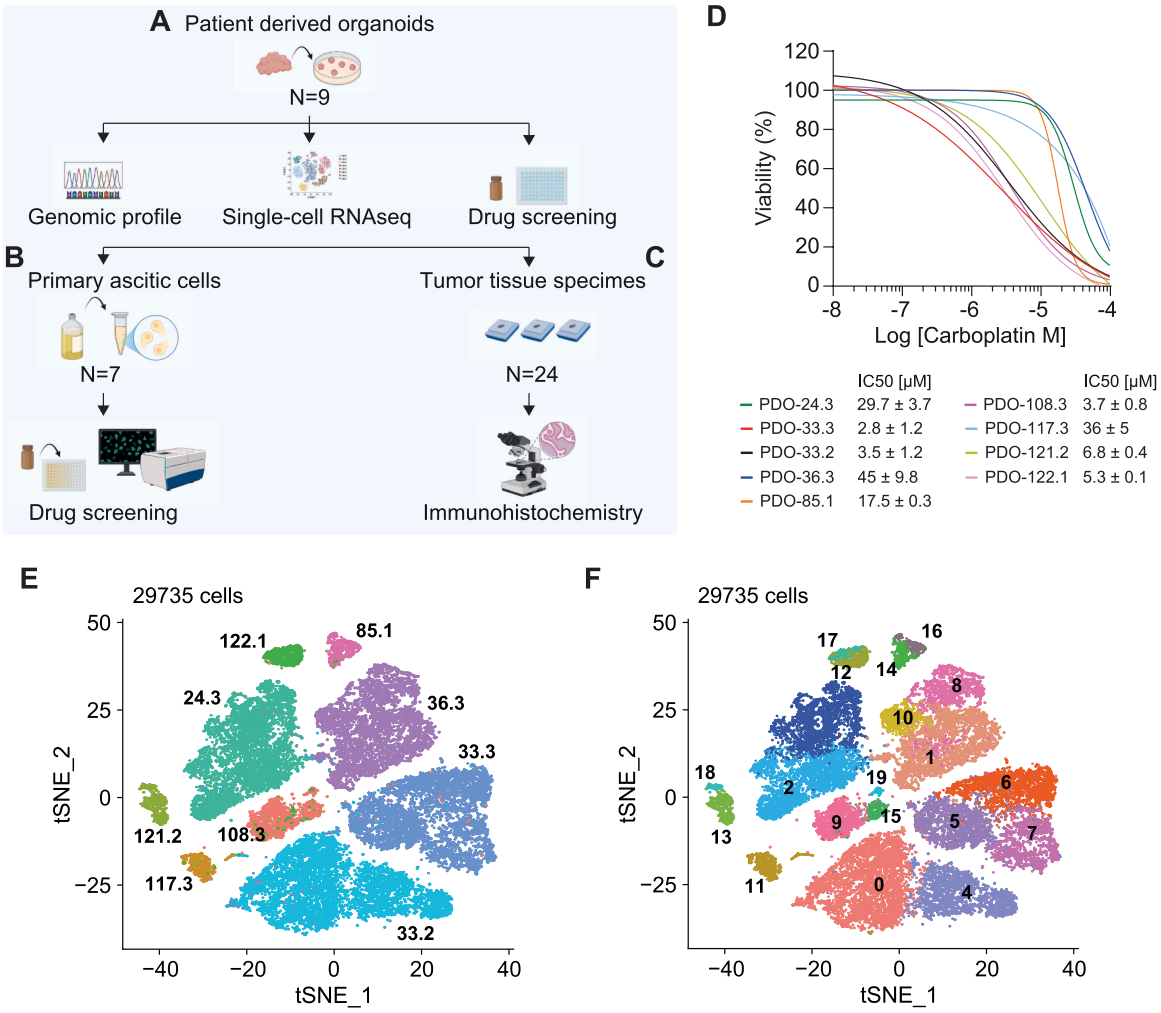

Fig. 1. PDOs retain patient-specific response to chemotherapy and genomic features of the original tumor. Scheme of the study workflow. (A) PDOs were subjected to: i) genomic profiling using the TruSight Oncology 500 panel, ii) single-cell transcriptomic analysis with the BD Rhapsody system, iii) drug screening in 96-well plates using CellTiter-Glo luminescent assay to assess viability after 5-day treatment. (B) scRNAseq analysis revealed transcriptional cluster signatures, which were compared to ascitic derived ovarian cancer spheroids (ADOCS). Ascitic fluid samples were processed to isolate tumor cells and generate ADOCS and spheroid cells were tested for sensitivity to cisplatin and Gboxin using the IncuCyte SX5 live-cell imaging system. (C) Expression of MHC-II proteins, identified in PDOs after NACT, was validated by immunohistochemistry on matched FFPE tumor tissues collected pre- and post-NACT from biopsies of 24 HGSOC patients. (D) Cytotoxic effects of Carboplatin on the indicated PDO lines. PDO cells were exposed to various concentrations of the drugs for 5 days and viability was evaluated by Cell Titer Glo 3D assay. IC_{50} values were determined from fitting curves using GraphPad Prism. Data in the graph are shown as the means ± SD from 3 independent experiments. (E) t-SNE showing clustering by PDO samples of PDOs as in B and additional five PDOs single cells (n = 29735) analyzed by scRNA-seq. (F) t-SNE embeddings showing the 20 distinct clusters identified from single cell analyses in the nine PDO analyzed in E.

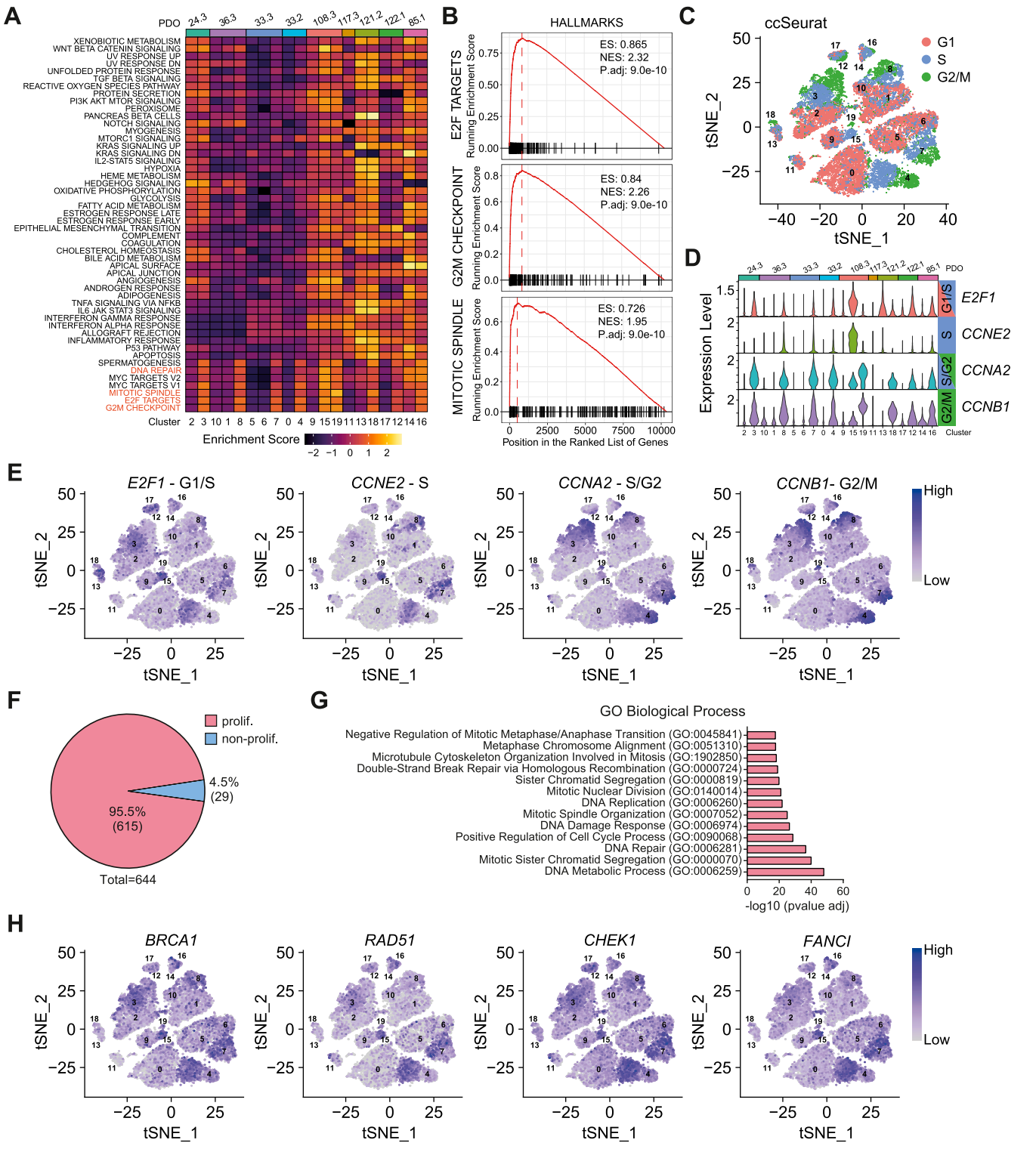

Fig. 2. Proliferative cells are a subpopulation of HGSOC PDOs featuring the expression of cell-cycle and DDR genes. (A) Heatmap showing the enrichment score of MSigDB hallmarks gene sets for each cluster identified from single-cell transcriptomic analyses. In red are highlighted hallmarks associated with a proliferative state and DNA damage repair. (B) Enrichment plot of E2F TARGETS, G2M CHECKPOINT and MITOTIC SPINDLE GSEA hallmarks. Enrichment score (ES), normalized enrichment score (NES) and adjusted *P*-value are shown. (C) t-SNE embeddings of cell distribution in G1, S, G2/M cell cycle phase measured using ccSeurat. (D) Violin plots showing average expression levels of *E2F1*, *CCNE2*, *CCNA2* and *CCNB1* genes in the indicated clusters of each PDO analyzed. (E) t-SNE embeddings of *E2F1*, *CCNE2*, *CCNA2* and *CCNB1* gene expression. (F) Pie chart showing percentages and numbers of genes whose expression is significantly enriched in proliferative (pink) or non-proliferative (light blue) clusters. (G) Gene ontology analyses of the biological processes significantly affected by upregulated genes in proliferative clusters. (H) t-SNE embeddings of *BRCA1*, *RAD51*, *CHEK1* and *FANCI* gene expression.

To gain a more comprehensive understanding of the transcriptomic signatures of HGSOC PDOs, we then searched for differentially expressed genes (DEGs; fold change ≥1.5; p-adj≤0.05) between the proliferative and non-proliferative clusters (Fig. 2F, Supplementary Table S2B). Consistent with the GSEA results (Fig. 2A,B and Fig. S3A), the genes upregulated in proliferative clusters were enriched in terms related to cell cycle (Fig. 2G, Fig. S3C). Furthermore, these clusters were significantly enriched for genes associated with DNA repair and the DDR (Fig. 2G), key processes triggered by platinum-based chemotherapy and whose alteration affects HGSOC prognosis and therapeutic strategies (Vanacker et al., 2021; Vergote et al., 2022a). This differential expression was confirmed by t-SNE clustering, showing that DDR genes were

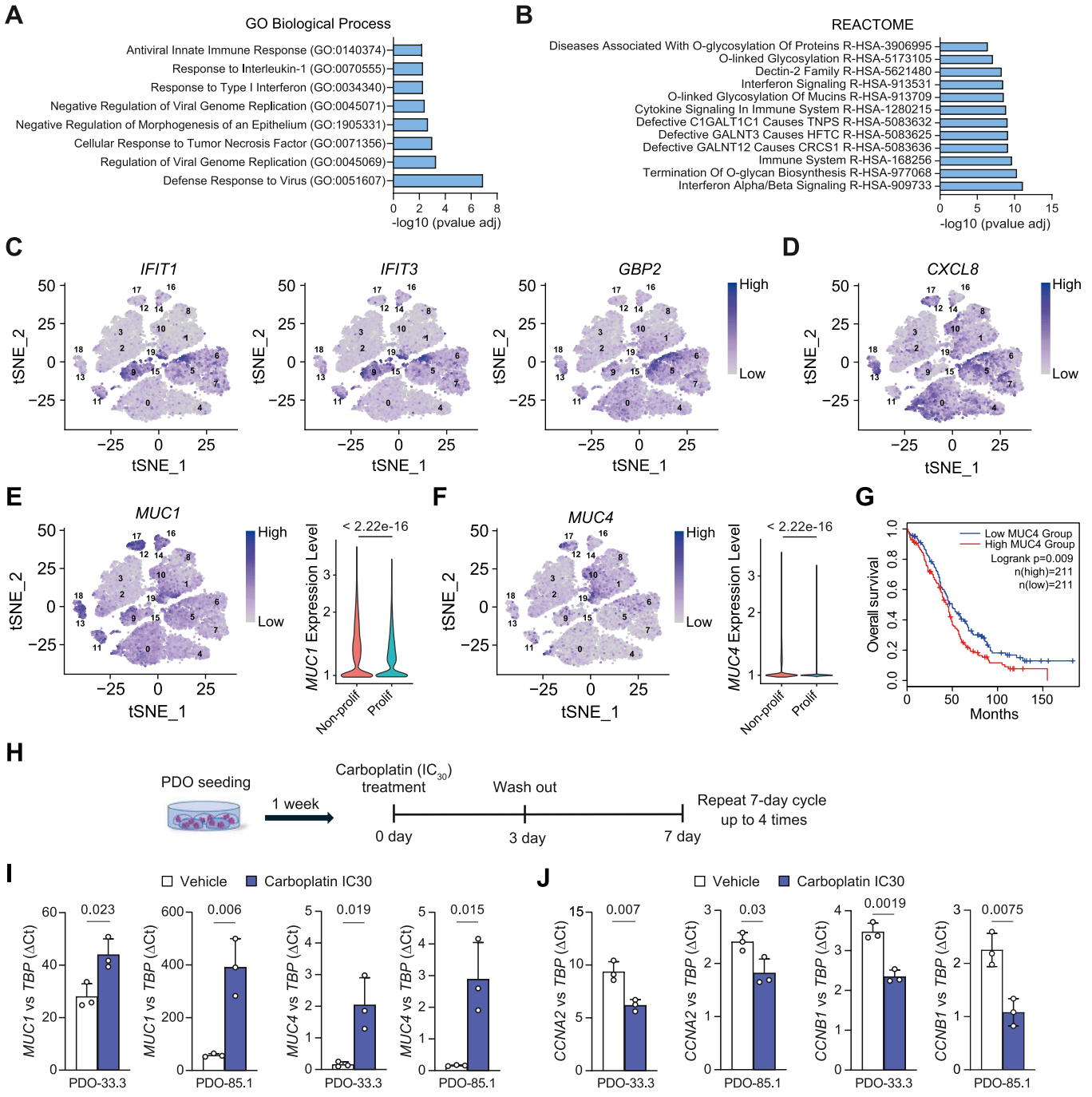

Fig. 3. Non-proliferative cell clusters feature the expression of inflammatory and O-glycan biosynthesis genes. (A, B) Gene ontology analyses of the biological processes (A) and REACTOME pathways (B) significantly enriched among the upregulated genes in non-proliferative clusters of HGSOC PDOs. (C) t-SNE embeddings of *IFIT1*, *IFIT3* and *GBP2* gene expression. (D) t-SNE embeddings of *CXCL8* gene expression. (E, F) t-SNE embeddings of *MUC1* (E) and *MUC4* (F) gene expression (left panel) and violin plots showing average expression levels of *MUC1* (E) and *MUC4* (F) in non-proliferative clusters respect to proliferative clusters (right panel). *P*-values were calculated by the Wilcoxon rank-sum test. (G) Kaplan–Meier curves comparing the overall survival of patients with high (red) or low (blue) expression of *MUC4* transcripts. *P*-value was calculated by the Logrank test. (H) Schematic representation of the timeline for *ex-vivo* chemotherapeutic treatment procedures. After seeding, PDOs were treated with IC_{30} concentration of carboplatin for 3 days followed by recovery for 4 days. This treatment schedule was repeated for 4 weeks. At the end, analysis of gene expression was evaluated by qPCR. (I, J) Bar graphs reporting the qPCR analyses of the *MUC1* and *MUC4* (I) or the *CCNA2* and *CCNB1* (J) transcripts relative to *TBP* in PDO-33.3 and PDO-85.1 treated or not with carboplatin, according to the timeline reported in H. Data represent the means ± SD from 3 independent experiments (unpaired *t* test).

expressed by proliferating (S and G2/M phases of the cycle), whereas they were clearly downregulated in non-proliferative cell clusters (Fig. 2H and Fig. S3D). Together, these analyses indicate that clusters of proliferative and non-proliferative cells co-exist in cultured HGSOC PDOs and that only the fraction of cells engaged in cell cycle progression is characterized by high expression of DDR genes.

Non-proliferative clusters of HGSOC PDOs feature inflammatory and O-glycan biosynthesis signatures

The non-proliferative clusters of HGSOC PDOs were significantly enriched in cancer hallmarks related inflammation (TNF-α signalling and IFN response) and hypoxia (Fig. S3A). These pathways were previously shown to characterize specific subpopulations of tumor cells from primary and metastatic sites (Vazquez-Garcia et al., 2022). However, the fold enrichment and statistical robustness of these pathways in non-proliferative clusters was limited (Fig. S3A). Likewise, t-SNE representation showed that TNFα pathway genes do not clearly separate proliferative and non-proliferative cells (Fig. S4A). The hypoxia signature was also not strongly upregulated in non-proliferative clusters. Indeed, while non-proliferative clusters 2, 5, 6, 9 and 14 showed a high hypoxic score, expression of hypoxia-related genes was also high in the proliferative clusters 7, 15 and 19 (Fig. S4B-E).

Analyses of biological processes and pathways enriched in the non-proliferative clusters retrieved defense against viruses and the type I IFN (IFNα/β) pathway (Fig. 3A,B). Nevertheless, t-SNE representation of genes in these pathways showed that they were strongly expressed only by some PDOs (PDO-33.3 and PDO-108.3), thus not representing a general feature of non-proliferative clusters (Fig. 3C). Likewise, *CXCL8* (encoding for interleukin 8) was not a strong marker of these clusters (Fig. 3D). Another pathway enriched in the non-proliferative clusters was O-glycan biosynthesis (Fig. 3B). Genes within this pathway, like *MUC1*, are being exploited as surface anchors to specifically deliver anticancer drugs in ovarian cancer (Basnet et al., 2024) and as circulating biomarker for detection of HGSOC in patients (Cooper et al., 2024). *MUC1* expression was higher, albeit not exclusive, in cells of the non-proliferative clusters with respect to the proliferative ones for each of the PDOs analyzed (Fig. 3E). Another interesting gene in this category is *MUC4*, which was recently reported to be highly expressed in the S100A9-positive ($S100A9^{+}$) subpopulation of cells present in both primary and metastatic HGSOC lesions and associated with poor overall survival in patients (Xu et al., 2024). We found that expression of *MUC4* is more restricted than that of MUC1 within the non-proliferative clusters (Fig. 3F), suggesting that it may mark a specific subpopulation of quiescent cells. Notably, high *MUC4* expression is significantly associated with worse prognosis in ovarian cancer patients (Fig. 3G), whereas that of *MUC1* or other genes in the O-glycan biosynthetic pathway and enriched in non-proliferative clusters of HGSOC PDOs is not (Fig. S4F).

Since platinum-based chemotherapy preferentially targets cells undergoing cell cycle progression, we asked whether it caused a proportional increase in the fraction of non-proliferative clusters. To test this hypothesis, we mimicked chemotherapeutic treatments by exposing PDOs to cycles of a sub-optimal dose (IC_{30}) of carboplatin (3 days) followed by recovery (4 days) for four consecutive weeks (Fig. 3H). Analysis by quantitative real time PCR (qPCR) indicated the upregulation of both *MUC1* and *MUC4* genes in PDO-33.3 and PDO-85.1 (Fig. 3I), which was paralleled by a significant reduction in the expression of markers of the proliferative clusters, such as *CCNA2* and *CCNB1* (Fig. 3J). These data suggest that only a fraction of HGSOC PDO cells is susceptible to inhibition of biological processes and pathways (i.e. cell cycle and DNA repair) that are targeted by chemotherapy, potentially leading to enrichment of non-proliferative clusters in tumors exposed to prolonged treatments. However, expression of MUC1 and MUC4 in non-proliferating HGSOC cells could be exploited in combination therapies with canonical chemotherapy.

Platinum resistant HGSOC are characterized by an OXPHOS signature

To investigate whether platinum resistance was associated with a specific transcriptional state in HGSOC PDOs, we compared the signatures of two platinum-sensitive (PDO-33.3, PDO-108.3) and two platinum-resistant (PDO-24.3, PDO-36.3) lines. GSEA of cancer hallmarks showed that platinum-sensitive PDOs are enriched in genes associated with mitotic, hypoxia and inflammatory pathways (Fig. 4A). On the other hand, the only signature enriched in the clusters of platinum-resistant PDOs was oxidative phosphorylation (OXPHOS) (Fig. 4A). The OXPHOS signature was enriched in both proliferative and non-proliferative clusters of platinum-resistant PDOs (Fig. S5A,B), suggesting that the metabolic switch to OXPHOS is a general feature that accompany chemoresistance in these tumors. Coherently, gene ontology (GO) analysis of the DEGs significantly upregulated in platinum-resistant PDOs retrieved all terms related to the mitochondrial respiratory chain (Fig. S5C,D). Likewise, the OXPHOS signature comprising all genes belonging to the five complexes (I to V) of the respiratory chain was significantly enriched in the platinum-resistant (PDO-24.3 and PDO-36.3) organoids (Fig. 4B,C). To validate these observations on an independent cohort, we analyzed single-cell transcriptomic data from a study that compared HGSOC samples taken before and after NACT (Zhang et al., 2022). Analysis of tumor epithelial cells from the pre-NACT samples of patients that resulted either sensitive or resistant to carboplatin-based chemotherapy confirmed the specific enrichment in the OXPHOS hallmark in platinum-resistant tumors (Fig. S5E-G). Moreover, the score of the OXPHOS signature was also significantly higher in platinum-resistant tumors with respect to platinum sensitive ones (Fig. S5H,I).

To directly test these computational results, we focused on the complex I *NDUFA3* and the complex V *ATP5F1E* genes, which were significantly upregulated in platinum-resistant PDOs (Fig. 4D). Analyses by qPCR confirmed the higher expression of these genes in platinum-resistant PDO-24.3 with respect to platinum-sensitive PDO-33.3 (Fig. 4E). A similar up-regulation was also observed for other genes involved in the mitochondrial respiratory chain (Fig. S5J,K). More importantly, PDO-24.3 exhibited increased sensitivity to treatment with the complex V inhibitor Gboxin (Fig. 4F), resulting in higher representation of small size organoids upon treatment with the drug (Fig. 4G,H). Lastly, analysis of all nine PDOs in our cohort confirmed that the OXPHOS score was inversely associated with sensitivity to carboplatin in these preclinical models (Fig. 4I, Fig. S5L).

The above-described findings suggest that HGSOC chemoresistance is associated with a metabolic switch in the glycolytic pathway. To orthogonally validate these observations, we isolated HGSOC cell spheroids developed from liquid biopsies of the ascitic fluid taken from seven chemo-naïve patients (Fig. 1B, Fig. 5A). Five of these primary tumor cell lines resulted highly sensitive to platinum treatment, which caused 70–80 % growth inhibition (Fig. 5B), whereas two of them were insensitive to the drug (Fig. 5C). Strikingly, platinum-sensitive ascitic cell lines resulted either insensitive to Gboxin (lines 312, 320 and 321) or grew better upon OXPHOS inhibition (lines 281 and 310; Fig. 5B). By contrast, growth of the two platinum-resistant ascitic cell lines was significantly reduced in the presence of Gboxin (Fig. 5C). Furthermore, representative OXPHOS genes were significantly more expressed in platinum insensitive ascitic cells (Fig. 5D). Collectively, these data support the notion that the metabolic switch to OXPHOS is a feature of platinum-resistant HGSOC, which in turn generates higher vulnerability to inhibitors of the mitochondrial respiratory chain.

NACT induces the expression of MYC and MHC-II genes in HGSOC

Next, we asked whether chemotherapy induced adaptive changes in the transcriptome of HGSOC cells. Comparison of the single-cell datasets of post-NACT PDO-33.2 and its parental pre-NACT PDO-33.3 identified 616 DEGs, with most of them (74 %) being upregulated in the post-

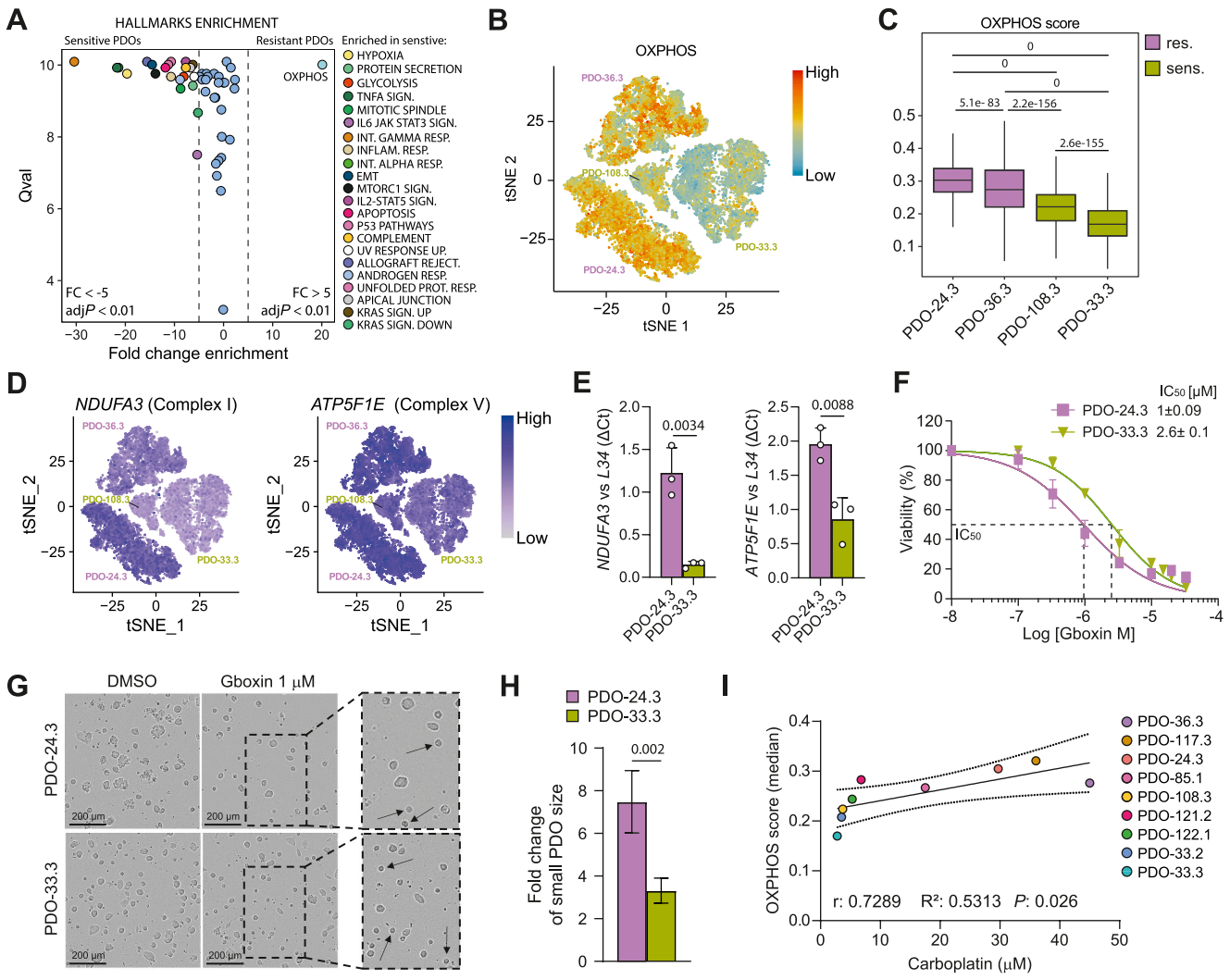

Fig. 4. Metabolic switch to OXPHOS is a feature of chemoresistance in HGSOC. (A) Volcano plot showing Qval output from SCPA plotted against MSigDB hallmarks gene sets measured as mean hallmark change in the comparison between chemo-resistant and chemo-sensitive PDOs. Blue points show significant hallmarks with no enrichment, and coloured points show significant hallmarks that also show enrichment. (B) t-SNE embeddings showing the OXPHOS score in the indicated chemo-resistant (purple) and chemo-sensitive (green) PDOs. (C) Box plots showing the distribution of OXPHOS score in the indicated chemo-resistant (purple) and chemo-sensitive (green) PDOs. Whiskers indicate 1.5 interquartile range, black lines represent median of values. *P*-values were calculated by the Wilcoxon rank-sum test. (D) t-SNE embeddings of *NUDFA3* and *ATP5F1E* gene expression. (E) Bar graphs of the qPCR analyses for the expression of the *NUDFA3* and *ATP5F1E* transcripts relative to *L34* in chemo-resistant PDO-24.3 and chemo-sensitive PDO-33.3. Data represent the means ± SD from 3 independent experiments (unpaired *t* test). (F) Cytotoxic effect of the complex V inhibitor Gboxin in PDO-24.3 and PDO-33.3. PDOs were treated with the indicated concentrations of Gboxin for 5 days. Living cells were measured using Cell Titer Glo 3D assay and IC_{50} values were determined from fitting curves using GraphPad Prism. (G) Representative brightfield images of the indicated PDOs plated in 96-well plate and treated with 1 μM Gboxin for 5 days (scale bar 200 μm). Insets show a magnified image with small size PDOs indicated by black arrows. (H) Bar graph reporting the fold change relative to quantification of small size PDOs in Gboxin-treated samples. Data in the graph represent the means ± SD from 3 independent experiments (unpaired *t* test). (I) Correlation between OXPHOS score and carboplatin IC_{50} in the indicated PDOs. The *r* value, *R2* value and *P* value were determined by Pearson correlation analysis.

NACT PDO-33.2 (Fig. 6A). GSEA showed that the OXPHOS hallmark is induced in the PDO developed after chemotherapy (Fig. 6B). Coherently, we observed a mild but significant increase in the score of the OXPHOS signature in the post-NACT PDO-33.2 (Fig. S6A) and in tumor cells of samples collected after NACT from an independent cohort (Fig. S6B,C). GSEA also identified MYC targets as an enriched cancer hallmark in the post-NACT PDO-33.2 (Fig. 6B). Moreover, query of the ChEA and ENCODE databases confirmed a highly significant enrichment for MYC targets among the up-regulated genes (Fig. S6D). MYC itself was upregulated in PDO-33.2 (Fig. S6E,F), which is likely responsible for the consequent induction of its target genes. Since high MYC expression is associated with worse prognosis in ovarian cancer patients (Cesari et al., 2023; Shen et al., 2022), our analyses suggest that NACT induces adaptive changes in HGSOC cells through the upregulation of genes (MYC and its targets) and metabolic pathways (OXPHOS) that support their viability upon genotoxic stress and may be crucial for development of recurrence.

Interestingly, genes of the major complex of histocompatibility type II (MHC-II) were also significantly enriched in the post-NACT PDO-33.2 (Fig. 6C, Supplementary Table S2C). MHC-II molecules are involved in antigen presentation by professional antigen presenting cells (APCs) (Klein and Petrozziello, 2025) and can also be expressed by some epithelial tumor cells (Liu et al., 2025). Notably, previous data reported the expression of the MHC-II molecules HLA-DMB and HLA-DR in a subset of HGSOC that displayed increased immune cell infiltration and improved prognosis (Callahan et al., 2008). The *HLA-DRA*, *HLA-DRB1* and *HLA-DPA1* genes were among the top-ranking DEGs in PDO-33.2 cells (Supplementary Table S2C), whereas they were detected at lower

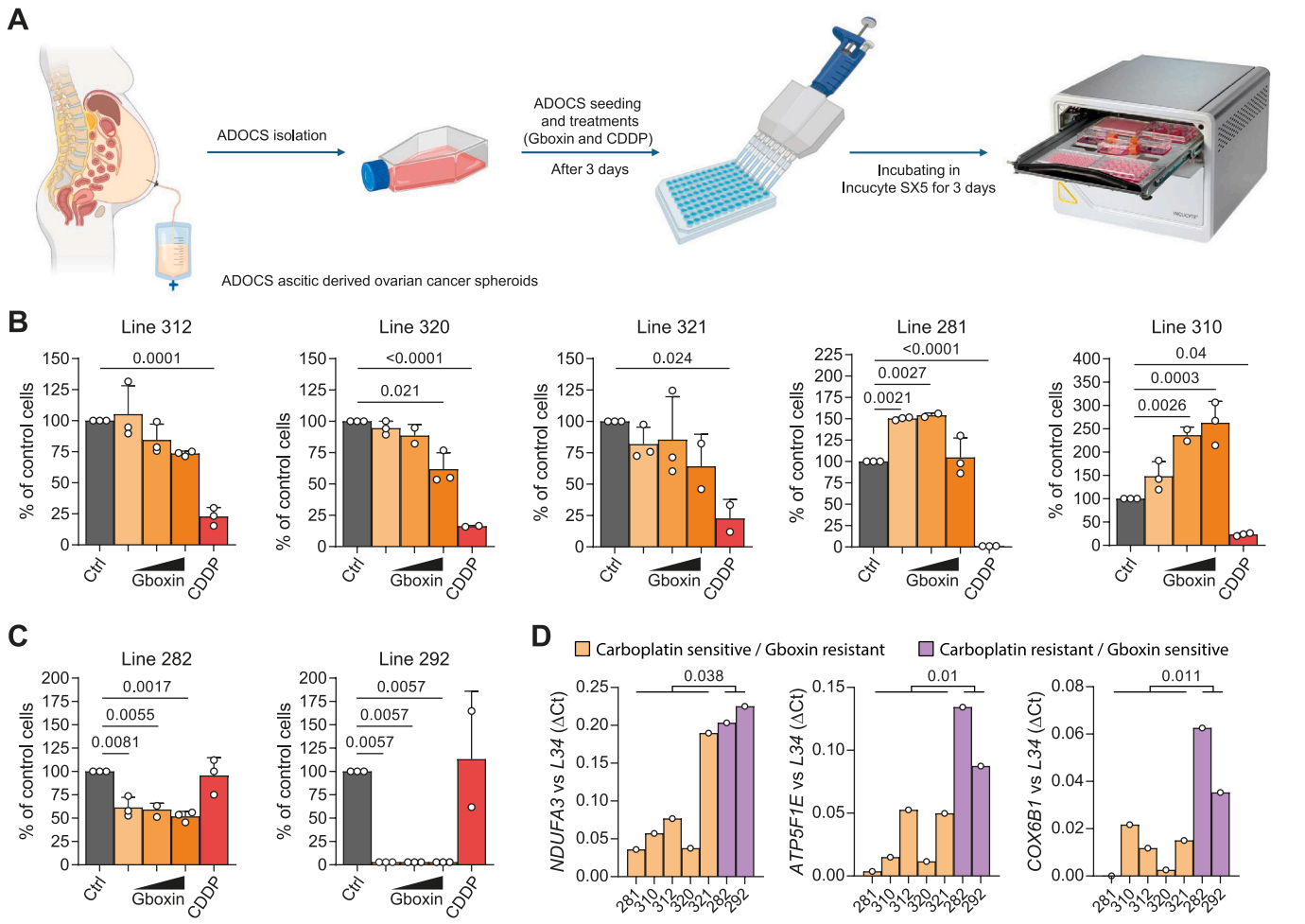

Fig. 5. Platinum resistant ascitic tumor cells are sensitive to oxidative phosphorylation inhibition. (A) Scheme of the procedure for ADOCS isolation and subsequent treatments. (B, C) Effects of Gboxin on the indicated platinum-sensitive (B) and platinum-resistant (C) ADOCS lines. Dissociated ADOCS cells were exposed to Cisplatin (25 μM) and Gboxin (0.3, 1, 3.3 μM) for 3 days and analyzed using the IncuCyte SX5 Live-content imaging system. The confluence (area) of adherent cells was measured, and results are expressed as percent of control. Data in the graph represent the means ± SD analyzed by one-way analysis of variance (ANOVA). (D) Bar graphs of qPCR analyses of the expression of *NDUFA3*, *ATP5F1E* and *COX6B1* transcripts relative to *L34* in the indicated ADOCS lines and groups. *P* values were determined by unpaired *t* test.

levels by only a minority of cells in PDO-33.3 (Fig. 6D). Expression of *CIITA*, which encodes for the transcriptional activator of MHC-II genes, was also upregulated in PDO-33.2 (Fig. 6D and Fig. S6G). Furthermore, analysis of pre- and post-NACT HGSOC cells from a separate cohort (Zhang et al., 2022) also showed up-regulation of MHC-II genes after chemotherapy (Fig. 6E-G; Fig. S6H-J). Importantly, up-regulation of MHC-II genes was also observed in the pre-NACT PDO-33.3 and the PDO-85.1 after four weeks of treatment with cycles of carboplatin ex-vivo (Fig. 6H,I), indicating that it represents a direct response of HGSOC cells to chemotherapy.

To validate these findings at the protein level, we analyzed specimens from a cohort of HGSOC patients (n = 24) undergoing IDS after NACT (Fig. 1C). Strikingly, immunohistochemistry analysis with a pan-HLA-DR antibody showed a marked up-regulation of MHC-II molecules in most patients (Fig. 6J,K), indicating that single-cell transcriptomic analysis of HGSOC PDOs is also predictive of tumor response *in vivo*. Moreover, this response was associated with increased immune cell recruitment in post-NACT HGSOC tissues (Fig. 6L,M). Lastly, we also found a significant correlation between HLA-DR expression and $CD3^+$ immune cell infiltration in naïve HGSOC samples (Fig. 6N,O), suggestive of a causal relationship between the two events.

Discussion

HGSOC is characterized by high molecular and cellular heterogeneity, which negatively affects the response to treatments (Veneziani et al., 2023). To further investigate this feature of HGSOC, we developed PDO lines from biopsies of patients who did or did not experience a positive response (PFI>6 months) to platinum-based chemotherapy. Although some patients were also treated with Bevacizumab as maintenance treatment, this drug did not affect the PFI nor the platinum free survival (PFS) in HGSOC patients (Burger et al., 2011; Perren et al., 2011), suggesting that it unlikely represents a confounding effect for the platinum response. Patient HGSOC-33 underwent NACT followed by IDS and we were also able to develop a PDO from the post-NACT biopsy. As previously observed by single-cell sequencing of primary HGSOC biopsies (Vazquez-Garcia et al., 2022), PDO cells showed transcriptome signatures that are highly patient specific. However, we were also able to identify two or three subclusters of cells in eight of the nine PDOs used in this study. Thus, PDOs comprise cells exhibiting significantly different transcriptional states, indicating that intra-tumor cell heterogeneity is also maintained in these organoid cultures. PDOs comprised clusters of proliferating and non-proliferating cells. Importantly, *ex-vivo* mimicking of platinum-based regimen caused an altered balance between these two subpopulations, with enrichment in markers of the non-proliferative

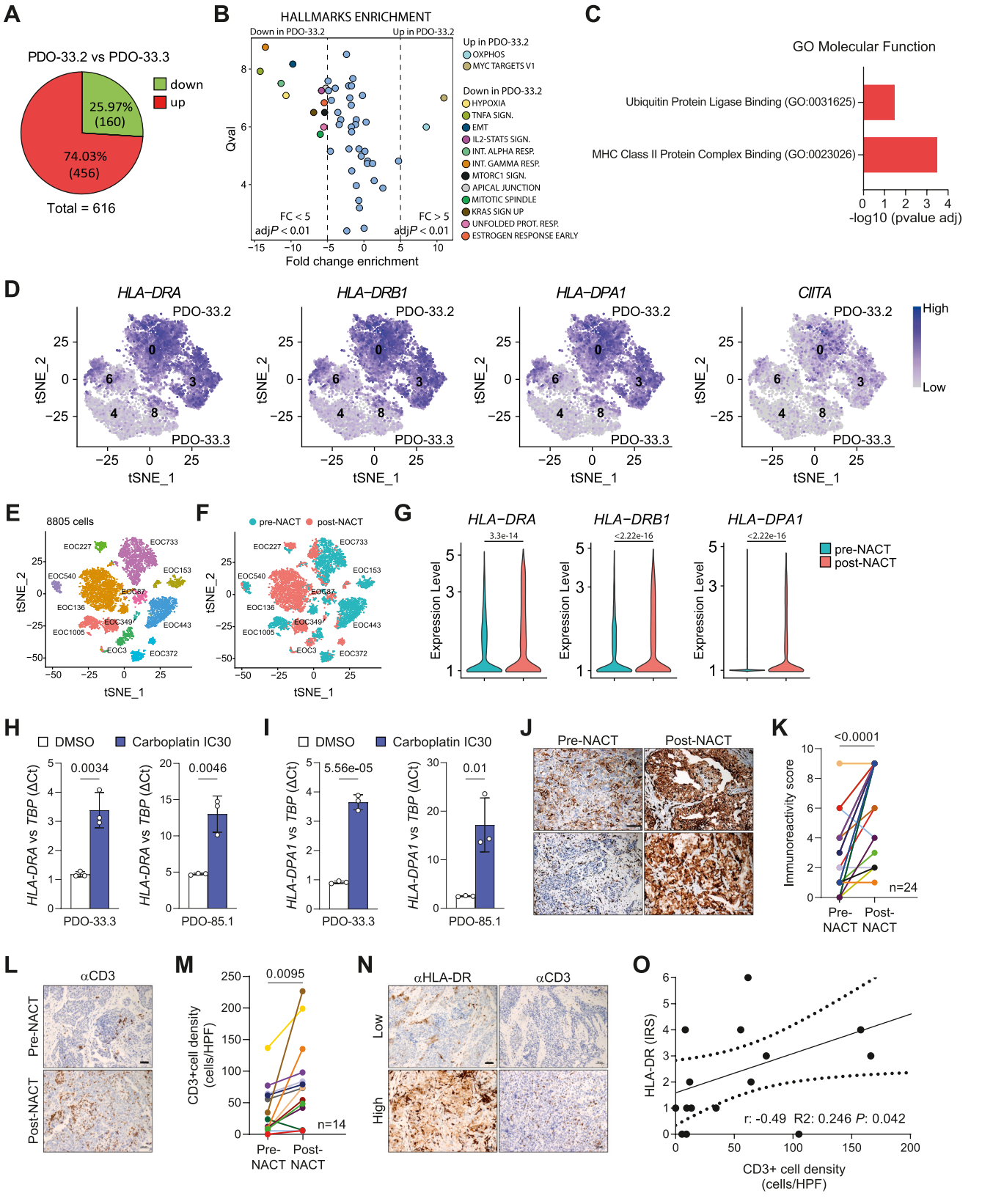

(caption on next page)

Fig. 6. NACT induces the expression of *MYC* and *MHC-II* genes in HGSOC. (A) Pie chart showing the genes whose expression is either up- (red) or down-regulated (green) in post-NACT PDO-33.2 respect to pre-NACT PDO-33.3. (B) Volcano plot showing Qval output from SCPA plotted against MSigDB hallmarks gene sets measured as mean hallmark change when comparing post-NACT PDO-33.2 to pre-NACT PDO-33.3. Blue dots show significant hallmarks with no enrichment; coloured dots show significant hallmarks that also show enrichment. (C) Gene Ontology analyses of the molecular functions significantly affected among the upregulated genes in post-NACT PDO-33.2. (D) t-SNE embeddings of *HLA-DRA*, *HLA-DRB1*, *HLA-DPA1* and *CIITA* gene expression. (E) t-SNE showing clustering by patient sample of HGSOC epithelial cells (n = 8805) analyzed by scRNA-seq from GSE165897 dataset. (F) t-SNE representation as in B annotated with colours corresponding to pre-NACT (cyan) and post-NACT (pink) samples. (G) Violin plots showing average expression levels of *HLA-DRA*, *HLA-DRB1* and *HLA-DPA1* transcripts in pre-NACT (cyan) and post-NACT (pink) samples. *P*-values were calculated by the Wilcoxon rank-sum test. (H, I) Bar graphs showing the qPCR analyses of the expression of *HLA-DRA* (H) and *HLA-DPA1* (I) transcripts relative to *TBP* in the indicated PDOs treated as in Fig. 3I. Data in the graph represent the means ± SD from 3 independent experiments (unpaired *t* test). (J) Representative IHC of HLA-DR in matched pre-NACT and post-NACT tissues from two representative patients with HGSOC. Scale bar: 50 μm. (K) Immunoreactivity score (IRS) measured from IHC analyses of HLA-DR as in (J) in matched pre-NACT and post-NACT from 24 patients with HGSOC (paired *t* test). (L) Representative sections of CD3 immunohistochemistry in pre- and post-NACT specimens from two patients affected by HGSOC. Magnification 20 × . (M) Lymphocytes density evaluated from IHC staining in matched pre-NACT and post-NACT from 14 patients with HGSOC (paired *t* test). (N) Representative pictures for clinical samples of untreated HGSOC showing low (upper panels) and high (lower panels) immunohistochemical staining of CD3 and HLA-DR. Magnification 20 × . (O) The Pearson rank correlation between HLA-DR IRS and $CD3^+$ cells density (cells/HPF) in samples from untreated HGSOC patients (n = 17, $P = 0.042$).

clusters. A similar depletion in mitotic genes was previously observed by bulk RNA sequencing of formalin fixed paraffin embedded (FFPE) samples collected from patients before and after chemotherapy (Javellana et al., 2022), supporting the clinical reliability of our PDO-based model. Our results are also in line with the previously reported plasticity of the transcriptional state of HGSOC cells, which were shown to change molecular phenotype under the pressure of chemotherapy (Arend et al., 2018; Javellana et al., 2022). Notably, DDR genes were mainly expressed in the proliferative clusters of our cohort of PDOs. Thus, since chemotherapy for HGSOC is based on disruption of DNA integrity by carboplatin and of the mitotic spindle by paclitaxel, it is conceivable that only the subgroup of cells undergoing cell cycle progression is susceptible to treatments. In this scenario, we propose that genes enriched in the non-proliferative clusters identified by our study, such as *MUC1* and *MUC4*, may represent valuable markers of treatment response and of the presence of surviving cells that are not targeted by platinum-based chemotherapy. Notably, MUC1 acts as a tumor-associated antigen and is expressed in 70 %–90 % of ovarian cancers (Lan et al., 2022). Recently, this transmembrane glycoprotein was exploited to specifically deliver an oncolytic virus to patient-derived ovarian cancer xenografts, causing tumor remission (Basnet et al., 2024). Hence, our findings suggest that markers of non-proliferative cellular subclusters could be exploited to develop treatments that also target the non-dividing HGSOC cells present in the bulk of tumor.

OXPHOS was the only hallmark upregulated in the intrinsically chemotherapy-resistant tumors (HGSOC-24 and HGSOC-36). We validated this observation in an independent cohort of HGSOC samples that were previously analyzed by single-cell RNA sequencing (Zhang et al., 2022), supporting the reliability of our analysis. The OXPHOS signature of PDOs and primary HGSOC tumors was inversely correlated with the sensitivity to carboplatin, suggesting that it represents a reliable marker of chemotherapy outcome. Of note, the OXPHOS signature was upregulated in both proliferative and non-proliferative clusters of platinum-resistant PDOs. Thus, this metabolic route could represent a valuable therapeutic target for chemoresistant HGSOC. In support of this hypothesis, proliferation of both platinum-resistant PDOs and primary HGSOC cells isolated from ascites were significantly more sensitive to the OXPHOS inhibitor Gboxin than platinum-sensitive ones. Coherently, platinum-resistant ovarian cancer cell lines were recently shown to develop an addiction to OXPHOS (Ponton-Almodovar et al., 2025; Udumula et al., 2024). Furthermore, it was proposed that mesenchymal stem cells associated to the tumor were capable to donate mitochondria to ovarian cancer cells, thus promoting the OXPHOS metabolic route, tumor cell heterogeneity and resistance to chemotherapy (Frisbie et al., 2024). Together, these results highlight OXPHOS as a metabolic vulnerability that could be targeted in platinum-resistant HGSOC.

Recent analyses of primary HGSOC specimens collected before and after chemotherapy from the same patients showed that treatments mainly induce transcriptome changes in the tumor, whereas genomic mutations did not show consistent patterns (Javellana et al., 2022). Our analyses of the transcriptome of pre- and post-NACT PDOs generated from the same patient (HGSOC-33) showed the chemotherapy-associated induction of OXPHOS genes. Furthermore, we validated the upregulation of the OXPHOS signature also in post-NACT tumor cells from an independent cohort of HGSOC patients (Zhang et al., 2022). Beside OXPHOS, the post-NACT PDO-33.2 also featured the upregulation of MYC and MYC target genes. The oncogene MYC is frequently amplified or overexpressed in HGSOC and its high expression predicts poor prognosis (Cesari et al., 2023; Shen et al., 2022). This observation further supports the reliability of our PDO platform for prediction of phenotypic features of HGSOC. In this regard, we also found a strong and highly selective up-regulation of MHC-II molecules in the post-NACT PDO-33.2 and in post-NACT tumor samples. Recent data suggest that reduced expression of MHC-II genes in HGSOC exhibiting whole-genome duplication is associated with worse clinical outcome in HGSOC, possibly by enabling immune escape (Burdett et al., 2024). On the other hand, up-regulation of specific MHC-II molecules in tumor cells was associated with higher immune cell infiltration and better prognosis in HGSOC patients (Callahan et al., 2008). Accordingly, increased tumor-infiltrating cytotoxic $CD8^+$ T cells is associated with favorable prognosis in HGSOC (Ovarian Tumor Tissue Analysis et al., 2017) and other tumors (Liu et al., 2025). We found that MHC-II expression was associated with increased immune cell recruitment in the tumor and that both HLA-DR and immune cell infiltration were significantly increased in primary tissue of patients exposed to NACT. Nevertheless, since another study showed that MHC-II upregulation promoted the recruitment T regulatory cells in the tumor and immune evasion in HRD ovarian cancers (Luo et al., 2024), the phenotypic features of the infiltrating immune cells should be assessed carefully.

The generally improved clinical outcome associated with up-regulation of MHC-II molecules by tumor cells was proposed to be related with a stronger anti-tumor immune reaction triggered by tumor antigen presentation. In support of this hypothesis, MHC-II expression was positively correlated with anti-PD-1 immunotherapy response in multiple cancer types (Liu et al., 2025). Since clinical trials with immunotherapies were largely unsuccessful in HGSOC (Kandalaft et al., 2022), the possibility to convert immunologically cold HGSOC into immune-responsive tumors by enhancing the expression of MHC-II molecules is clinically attractive. Herein, we found that the up-regulation of MHC-II molecules in post-NACT PDO-33.2 was a direct effect of chemotherapy, as it could be recapitulated *ex-vivo* by mimicking a platinum-based regimen on PDOs derived from chemotherapy-naïve tumors. Interestingly, carboplatin induced the expression of classical MHC-II molecules normally expressed by professional APCs (HLA-DRA/HLA-DRB), as well as of broader (HLA-DP/HLA-DQ) and non-classical (HLA-DM/HLA-DO) MHC-II molecules. These results indicate that tumor cells mount a general antigen-presenting response upon chemotherapeutic treatment. More importantly, we also observed

a marked and highly significant up-regulation of HLA-DR molecules in a validation cohort of post-NACT biopsies with respect to matched pre-NACT biopsies. Given the positive correlation between MHC-II expression in tumor cells and clinical response to immunotherapies (Liu et al., 2025), our findings may pave the ground for evaluation of sequential regimens including immune checkpoint inhibitors after initial cycles of platinum-based chemotherapy.

Materials and methods

Patient-derived organoids

We enrolled 100 HGSOC patients in the study over a 5-year period. In total, we developed 35 PDO lines (overall success rate of 35 %). 23 PDO lines could only be maintained for few passages (3−8) and with limited expansion, thus they were not considered suitable for this study. Of the 12 long-term PDO lines, 9 were employed for the subsequent analyses. PDOs were generated from HGSOC biopsies as described (Cesari et al., 2023). Tissues placed in 60 mm Petri dishes containing AdDF+ ++ culture medium (Advanced DMEM/F12 containing 1x Glutamax, 10 mM HEPES and antibiotics) were minced by surgical blades into small fragments and digested in 10 ml AdDF+ ++ supplemented with 5 μM RHO/ROCK pathway inhibitor (Y-27632, Tocris) containing 2 mg/ml Collagenase IV (ThermoFisher Scientific) on an orbital shaker at 37 °C for 1 h, as previously described (Cesari et al., 2023). Cells were embedded in BME (Cultrex growth factor reduced BME type 2, Trevigen) on ice and 40 μl drops of BME cell suspension were allowed to solidify to a pre-warmed 24 well suspension culture plates (Greiner) and then placed at 37°C in humidified air containing 5 % CO2. Organoid culture medium was AdDF+ ++ culture medium supplemented with EGF (100 ng/ml), A83–01 (0.5 μM), B27 (1X) and N2 (1X) supplement, Y-27632 (9 μM), Nicotinamide (1 mM) and Primocin. Organoids were passaged every 1–4 weeks by incubation with Cultrex Organoid Harvesting Solution for 45 min at 4 °C to digest the BME as described (Cesari et al., 2023). Genomic analysis of PDOs and original tumors were carried out using the TruSight Oncology (TSO) 500 by Next Generation Sequencing technology (Illumina Inc.).

Single-cell sequencing and data processing

Single-cell sequencing was performed on 9 PDOs, and the clinical information is given in Fig. 1D and Supplementary Table S3. Single-cell analyses were performed with the microwell-based Rhapsody Single-Cell Analysis System (#633701, BD). PDOs were enzymatically dissociated into a single cell suspension using Triple Express (Gibco) at 37°C and labelled with sample tags using the Human Single-Cell Multiplexing Kit (#633781, BD). mRNA library and the SampleTag library were prepared using the Rhapsody Cartridge kit (#633733, #664887, BD), the Rhapsody Whole Transcriptome Assay Analysis Amplification Kit (#633801, BD), diluted to 4 nM and multiplexed for paired-end sequencing on an Illumina NovaSeq6000 (Illumina). FASTQ files with raw sequencing reads were processed with the standard BD Rhapsody Whole Transcriptome Assay Analysis Pipeline on Seven Bridges (https://www.sevenbridges.com), which included filtering by reads quality, annotating reads, annotating molecules, determining putative cells, and generating single-cell expression matrix. We excluded cells with $<$ 1500 detectable genes, $>$ 120,000 unique molecular identifiers, $>$ 45 % mitochondrial transcripts, and $>$ 30 % ribosomal transcripts following the Seurat pipeline (v4.3.0). Both multiplets and undetermined cells were excluded from analysis. Expression data was normalized to the total expression, multiplied by a scaling factor of 10,000, and log-transformed. Cell types were annotated by using a combination of the built-in reference datasets of known cell types of SingleR package (v1.6.21), by validation with well-known HGSOC markers (Croft et al., 2024; Hao et al., 2021a; Santoro et al., 2025) and by querying the CellMarker 2.0 database for ovary-cancer cells. The top 2000 highly variable genes based on the variance stabilizing transformation function *FindVariableFeatures* within Seurat were selected for canonical correlation analysis as an initial dimensional reduction. The dimensionality of the scaled data matrix was further reduced to project the cells in two-dimensional space using principal component analysis, and the top 30 principal components were included in a t-SNE dimensionality reduction. The resulting principal components were also used as a basis for partitioning the dataset into clusters using a shared nearest neighbor (SNN) modularity graph and a resolution of 0.5. Top 10 markers from each cluster were selected to create the heatmap and violin plots. Cell cycle assignment was performed using the *CellCycleScoring* function in Seurat (ccSeurat) and by calling *cc.genes.updated.*2019 dataset of G2/M and S phase well-known markers (Hao et al., 2021b). Gene set enrichment analysis (GSEA) heatmap for each cluster was performed with the *enrichIt* function of escape R package (v1.9.0) using the 50 hallmark gene sets in the MSigDB databases and single-cell GSEA method.

Differential gene expression between clusters was analyzed with the *FindMarkers* function in Seurat (min.pct=0.25, min.diff.pct=0.25) and p-value was calculated using the Wilcoxon rank-sum test with Bonferroni correction. Genes with p-value$\leq$ 0.05 and fold change$\geq$ 1.5 were considered and used for GSEA, Gene Ontology (GO) and REACTOME enrichment analysis using the enrichR R package (v3.2). Comparisons for differential enrichment of hallmark gene sets between clusters were performed using the *compare_pathways* function within SCPA R package (v1.6.0). Quantification and scoring of single cell metabolic pathway gene sets were performed using scMetabolism R package (v0.2.1). Data were processed by using ggplot2 (v3.5.0), dittoSeq (v1.4.4), ggpubr (v0.4.0), ggsignif (v0.6.3), ComplexHeatmap (v2.8.0), RColorBrewer (v1.1–2) and cowplot (v1.1.1). For scRNA-seq data of a total of 22 matched pre- and post-NACT HGSOC tissue specimens (GSE165897 - (Zhang et al., 2022)) the Seurat package was used to exclude cell with $<$ 500 detectable genes, $<$ 500 unique molecular identifiers and $>$ 12 % mitochondrial transcripts, integrate data and subset for epithelial cells. Subsequent differential gene expression and pathway analyses were performed as describe above.

RNA extraction and PCR analysis

Total RNA was extracted using RNA Mini Kit (Geneaid) and 1 μg of RNA was retro-transcribed with oligo-dT oligonucleotides, using M-MLV reverse transcriptase (Promega). 20 ng of cDNA was used as template for PCR (GoTaq, Promega). Quantitative real-time PCRs (qPCR) were performed using LightCycler 480 SYBR Green I Master and the LightCycler 480 System (Roche), according to the manufacturer's instructions. Control reactions omitting M-MLV reverse transcriptase were also carried out. PCR oligonucleotides are listed in Table S3.

Cell viability assay

Dissociated PDOs were resuspended in 2 % BME/growth medium and seeded in 100 μl volume on BME pre-coated 96-well plates. After 24 h, the cells were treated with the indicated drugs for 5 days and viability was determined by CellTiter-Glo® Luminescent Cell Viability Assay (Promega) using a microplate reader (Spark, Tecan). Assays were performed on re-formed organoids of small volumes, which reflect the response of a 3D tumor structure. Cytotoxicity was determined relative to the control cells exposed to vehicle and analyzed using GraphPad Prism 9 (GraphPad Software). Drug dose-response curves were visualized using linear regression analysis (setting: log(inhibitor) versus normalized response). Half-maximal inhibitory concentration (IC_{50}) values were determined from fitting curves. PDOs were classified as small, medium or large based on their diameter measured manually with ImageJ software.

Immunohistochemistry analysis

Within the institutional Histopathology Biobank, 24 matched pairs of tumor tissue specimens collected before and after NACT were selected. Histological sections (5 μm) of paraffin-embedded tissues were stained with primary monoclonal mouse anti-human HLA-DP, DQ, DR antibody (Clone CR3/43, F081701–2, DAKO/AGILENT) and monoclonal rabbit anti-CD3 (clone 2GV6, ROCHE Ventana Diagnostic) antibody. The immunostaining was performed on the Bond III automated immunostainer (Leica Microsystems). Appropriate positive and negative controls were included. The selected antibodies are well-established in the diagnostic routine laboratory; signals were clearly visible and captured by ordinary light AxioPhot microscope (Zeiss).

The status of antigen expression was semi-quantitatively evaluated by two investigators in blind. Regarding HLA-DR staining, an immunohistochemical score (IRS, 0–9) was calculated by multiplying the two factors obtained following categorization of the percentage of stained cells (1 =1–30 %; 2 =31–60 %; 3 =61–100 %) and the intensity of staining (1 =weak staining; 2 =moderate staining; 3 =strong staining).

Intratumoral lymphocytes were defined as those in direct contact with tumour cells or within the tumour itself. Lymphocyte densities were assessed by counting the number of intratumoral CD3 positive cells that were present in regions with highest densities, hotspots. Four 400 × high-power fields (HPFs) (×400 objective magnification, high-power field area= 0.24 mm2) were evaluated and the lymphocytes density was then expressed as mean number of CD3 + cells per HPF (CD3/HPF).

Isolation and analysis of ascitic cells

Ascitic fluid was centrifugated and the pellet washed by PBS; after centrifugation the pellet was resuspended in Red Blood Cell Lysis Buffer (Roche) and incubated for 10 min to reduce the blood cell contamination. Cells were centrifugated and the pellet resuspended in OCMI medium (Ovarian Cancer Modified Ince Medium) supplemented with 10 ng/ml EGF, 20 μg/ml insuline, 500 ng/ml hydrocorstisone, 25 ng/ml colera toxin, 5 % FBS, 2 mM Glutamine, and Penicillin–Streptomycin (Ince et al., 2015). Ascitic derived ovarian cancer spheroids (ADOCS) were isolated by culturing for 3 days under restrictive conditions, in Ultra Low Attachment Plates (Corning). Dissociated cancer cells were then seeded in 96-well plate in adhesion condition and were treated with 25 μM Cisplatin and Gboxin (0.3, 1, 3.3 μM) for 3 days; plates were incubated into IncuCyte SX5 Live-content imaging system at 37 °C with 5 % CO_2. Three wells (nine fields/well) for each condition were analysed by measuring the confluence of adherent cells. Cell-covered area at each time point was normalized to the starting value in the same well after seeding (T_0).

Statistical analyses

Cell proliferation data were analyzed by one-way analysis of variance (ANOVA), using Tukey's multiple comparison test to determine if significant differences existed between groups. qPCR and PDO size data were evaluated by the two-tailed unpaired Student's *t*-test. All data are reported as mean ± SD ($n \geq 3$) and statistical analyses were performed using the GraphPad Prism10 Software.

CRediT authorship contribution statement

Alessia Piermattei: Resources, Investigation. **Angelo Minucci:** Resources, Investigation. **Eleonora Kristina Scarpone:** Methodology, Investigation, Formal analysis. **Eleonora Cesari:** Methodology, Investigation, Formal analysis. **Claudio Sette:** Writing – original draft, Supervision, Resources, Project administration, Methodology, Funding acquisition, Conceptualization. **Roberta Mastrantonio:** Methodology, Investigation, Formal analysis. **Giovanni Scambia:** Supervision, Resources, Funding acquisition, Conceptualization. **Alessandra Ciucci:** Writing – original draft, Visualization, Methodology, Investigation, Formal analysis, Data curation, Conceptualization. **Camilla Nero:** Writing – original draft, Supervision, Resources, Funding acquisition, Conceptualization. **Christian Corti:** Methodology, Investigation, Formal analysis. **Anna Fagotti:** Resources. **Luca Tamagnone:** Supervision, Resources, Funding acquisition, Conceptualization. **Marco Pieraccioli:** Writing – original draft, Visualization, Software, Investigation, Formal analysis, Data curation, Conceptualization. **Andrea Urbani:** Supervision, Resources. **Floriana Camarda:** Visualization, Data curation.

Ethics approval and consent to participate

Tumour biopsies were collected, under informed consent, from patients treated at Fondazione Policlinico A. Gemelli IRCCS (FPG), Rome, Italy. The protocol was approved by the Institutional Review Board (ClinicalTrial.gov ID: NCT06085404) and conducted in accordance with the Declaration of Helsinki. Relevant clinical data were collected and managed using REDCap electronic data capture tools at FPG (https://redcap-irccs.policlinicogemelli.it).

Funding

This work was supported by Ministry of University, PRIN-PNRR 2022 grant n. P2022NMJEC, Associazione Italiana Ricerca sul Cancro (AIRC) grant n. IG30651 and IG29255, the Italian Ministry of Health (Ricerca Corrente 2025) to IRCCS Fondazione Policlinico A. Gemelli, and the Università Cattolica del Sacro Cuore (Linea D1 and 5x1000). Università Cattolica del Sacro Cuore contributed to the funding of this research project and its publication.

Declaration of Competing Interest

The authors declare that they have no known competing financial interests or personal relationships that could have appeared to influence the work reported in this paper.

Acknowledgements

We acknowledge the contribution of the GSTeP Bioinformatics and Data Collection Research Core Facilities of FPG for collection of, respectively, sequencing and patients' data. We also wish to thank Dr. Enrica Martinelli for help in the immunohistochemistry analyses and all members of our laboratories for helpful discussions throughout the study. This article is dedicated to the memory of Prof. Giovanni Scambia, a great surgeon and scientist, and an inspiring friend and colleague.

Appendix A. Supporting information

Supplementary data associated with this article can be found in the online version at doi:10.1016/j.drup.2026.101354.

References

Arend, R.C., Londono, A.I., Montgomery, A.M., Smith, H.J., Dobbin, Z.C., Katre, A.A., Martinez, A., Yang, E.S., Alvarez, R.D., Huh, W.K., Bevis, K.S., Straughn, J.M., Jr, Estes, J.M., Novak, L., Crossman, D.K., Cooper, S.J., Landen, C.N., Leath, C.A., 3rd, 2018. Molecular response to neoadjuvant chemotherapy in high-grade serous ovarian carcinoma. Mol. Cancer Res. 16, 813–824. https://doi.org/10.1158/1541-7786.MCR-17-0594.

Basnet, S., Van der Heijden, M., Quixabeira, D.C.A., Jirovec, E., Gronberg-Vaha-Koskela, S.A.M., Clubb, J.H.A., Kanerva, A., Pakola, S., Haybout, L., Arias, V., Hemminki, O., Kudling, T., Zafar, S., Cervera-Carrascon, V., Santos, J.M., Hemminki, A., 2024. Overcoming effector T cell exhaustion in ovarian cancer ascites with a novel adenovirus encoding for a MUC1 bispecific antibody engager and IL-2 cytokine. Mol. Ther. 32, 3114–3127. https://doi.org/10.1016/j.ymthe.2024.06.029.

Burdett, N.L., Willis, M.O., Pandey, A., Twomey, L., Alaei, S., Australian Ovarian Cancer Study, G., Bowtell, D.D.L., Christie, E.L., 2024. Timing of whole genome duplication

is associated with tumor-specific MHC-II depletion in serous ovarian cancer. Nat. Commun. 15, 6069. https://doi.org/10.1038/s41467-024-50137-y.
Burger, R.A., Brady, M.F., Bookman, M.A., Fleming, G.F., Monk, B.J., Huang, H., Mannel, R.S., Homesley, H.D., Fowler, J., Greer, B.E., Boente, M., Birrer, M.J., Liang, S.X., Grp, G.O., 2011. Incorporation of Bevacizumab in the primary treatment of ovarian cancer. N. Engl. J. Med. 365, 2473–2483 https://doi.org/DOI 10.1056/NEJMoa1104390.
Callahan, M.J., Nagymanyoki, Z., Bonome, T., Johnson, M.E., Litkouhi, B., Sullivan, E.H., Hirsch, M.S., Matulonis, U.A., Liu, J., Birrer, M.J., Berkowitz, R.S., Mok, S.C., 2008. Increased HLA-DMB expression in the tumor epithelium is associated with increased CTL infiltration and improved prognosis in advanced-stage serous ovarian cancer. Clin. Cancer Res 14, 7667–7673. https://doi.org/10.1158/1078-0432.CCR-08-0479.
Cancer Genome Atlas Research, N., 2011. Integrated genomic analyses of ovarian carcinoma. Nature 474, 609–615. https://doi.org/10.1038/nature10166.
Cesari, E., Ciucci, A., Pieraccioli, M., Caggiano, C., Nero, C., Bonvissuto, D., Sillano, F., Buttarelli, M., Piermattei, A., Loverro, M., Camarda, F., Greco, V., De Bonis, M., Minucci, A., Gallo, D., Urbani, A., Vizzielli, G., Scambia, G., Sette, C., 2023. Dual inhibition of CDK12 and CDK13 uncovers actionable vulnerabilities in patient-derived ovarian cancer organoids. J. Exp. Clin. Cancer Res. 42, 126. https://doi.org/10.1186/s13046-023-02682-5.
Cooper, T.T., Dieters-Castator, D.Z., Liu, J., Siegers, G.M., Pink, D., Veliz, L., Lewis, J.D., Lagugne-Labarthet, F., Fu, Y., Steed, H., Lajoie, G.A., Postovit, L.M., 2024. Targeted proteomics of plasma extracellular vesicles uncovers MUC1 as combinatorial biomarker for the early detection of high-grade serous ovarian cancer. J. Ovarian Res. 17, 149. https://doi.org/10.1186/s13048-024-01471-8.
Croft, W., Pounds, R., Jeevan, D., Singh, K., Balega, J., Sundar, S., Williams, A., Ganesan, R., Kehoe, S., Ott, S., Zuo, J., Yap, J., Moss, P., 2024. The chromatin landscape of high-grade serous ovarian cancer metastasis identifies regulatory drivers in post-chemotherapy residual tumour cells. Commun. Biol. 7, 1211. https://doi.org/10.1038/s42003-024-06909-9.
Etemadmoghadam, D., Weir, B.A., Au-Yeung, G., Alsop, K., Mitchell, G., George, J., Australian Ovarian Cancer Study, G., Davis, S., D'Andrea, A.D., Simpson, K., Hahn, W.C., Bowtell, D.D., 2013. Synthetic lethality between CCNE1 amplification and loss of BRCA1. Proc. Natl. Acad. Sci. 110, 19489–19494. https://doi.org/10.1073/pnas.1314302110.
Frisbie, L., Pressimone, C., Dyer, E., Baruwal, R., Garcia, G., St Croix, C., Watkins, S., Calderone, M., Gorecki, G., Javed, Z., Atiya, H.I., Hempel, N., Pearson, A., Coffman, L.G., 2024. Carcinoma-associated mesenchymal stem cells promote ovarian cancer heterogeneity and metastasis through mitochondrial transfer. Cell Rep. 43, 114551. https://doi.org/10.1016/j.celrep.2024.114551.
Gorski, J.W., Ueland, F.R., Kolesar, J.M., 2020. CCNE1 amplification as a predictive biomarker of chemotherapy resistance in epithelial ovarian cancer. Diagnostics 10. https://doi.org/10.3390/diagnostics10050279.
Hao, Y., Hao, S., Andersen-Nissen, E., Mauck, W.M., 3rd, Zheng, S., Butler, A., Lee, M.J., Wilk, A.J., Darby, C., Zager, M., Hoffman, P., Stoeckius, M., Papalexi, E., Mimitou, E. P., Jain, J., Srivastava, A., Stuart, T., Fleming, L.M., Yeung, B., Rogers, A.J., McElrath, J.M., Blish, C.A., Gottardo, R., Smibert, P., Satija, R., 2021b. Integrated analysis of multimodal single-cell data. e3529 Cell 184, 3573–3587. https://doi.org/10.1016/j.cell.2021.04.048.
Hao, Q., Li, J., Zhang, Q., Xu, F., Xie, B., Lu, H., Wu, X., Zhou, X., 2021a. Single-cell transcriptomes reveal heterogeneity of high-grade serous ovarian carcinoma. Clin. Transl. Med. 11, e500. https://doi.org/10.1002/ctm2.500.
Hu, Z., Artibani, M., Alsaadi, A., Wietek, N., Morotti, M., Shi, T., Zhong, Z., Santana Gonzalez, L., El-Sahhar, S., Carrami, E.M., Mallett, G., Feng, Y., Masuda, K., Zheng, Y., Chong, K., Damato, S., Dhar, S., Campo, L., Garruto Campanile, R., Soleymani Majd, H., Rai, V., Maldonado-Perez, D., Jones, S., Cerundolo, V., Sauka-Spengler, T., Yau, C., Ahmed, A.A., 2020. The repertoire of serous ovarian cancer non-genetic heterogeneity revealed by single-cell sequencing of normal fallopian tube epithelial cells. e227 Cancer Cell 37, 226–242. https://doi.org/10.1016/j.ccell.2020.01.003.
Ince, T.A., Sousa, A.D., Jones, M.A., Harrell, J.C., Agoston, E.S., Krohn, M., Selfors, L.M., Liu, W., Chen, K., Yong, M., Buchwald, P., Wang, B., Hale, K.S., Cohick, E., Sergent, P., Witt, A., Kozhekbaeva, Z., Gao, S., Agoston, A.T., Merritt, M.A., Foster, R., Rueda, B.R., Crum, C.P., Brugge, J.S., Mills, G.B., 2015. Characterization of twenty-five ovarian tumour cell lines that phenocopy primary tumours. Nat. Commun. 6, 7419. https://doi.org/10.1038/ncomms8419.
Javellana, M., Eckert, M.A., Heide, J., Zawieracz, K., Weigert, M., Ashley, S., Stock, E., Chapel, D., Huang, L., Yamada, S.D., Ahmed, A.A., Lastra, R.R., Chen, M., Lengyel, E., 2022. Neoadjuvant chemotherapy induces genomic and transcriptomic changes in ovarian cancer. Cancer Res. 82, 169–176. https://doi.org/10.1158/0008-5472.CAN-21-1467.
Kandalaft, L.E., Dangaj Laniti, D., Coukos, G., 2022. Immunobiology of high-grade serous ovarian cancer: lessons for clinical translation. Nat. Rev. Cancer 22, 640–656. https://doi.org/10.1038/s41568-022-00503-z.
Kim, S.Y., van de Wetering, M., Clevers, H., Sanders, K., 2025. The future of tumor organoids in precision therapy. Trends Cancer 11, 665–675. https://doi.org/10.1016/j.trecan.2025.03.005.
Klein, L., Petrozziello, E., 2025. Antigen presentation for central tolerance induction. Nat. Rev. Immunol. 25, 57–72. https://doi.org/10.1038/s41577-024-01076-8.
Kopper, O., de Witte, C.J., Lohmussaar, K., Valle-Inclan, J.E., Hami, N., Kester, L., Balgobind, A.V., Korving, J., Proost, N., Begthel, H., van Wijk, L.M., Revilla, S.A., Theeuwsen, R., van de Ven, M., van Roosmalen, M.J., Ponsioen, B., Ho, V.W.H., Neel, B.G., Bosse, T., Gaarenstroom, K.N., Vrieling, H., Vreeswijk, M.P.G., van Diest, P.J., Witteveen, P.O., Jonges, T., Bos, J.L., van Oudenaarden, A., Zweemer, R. P., Snippert, H.J.G., Kloosterman, W.P., Clevers, H., 2019. An organoid platform for ovarian cancer captures intra- and interpatient heterogeneity. Nat. Med. 25, 838. https://doi.org/10.1038/s41591-019-0422-6.
Lan, Y., Ni, W., Tai, G., 2022. Expression of MUC1 in different tumours and its clinical significance (Review). Mol. Clin. Oncol. 17, 161. https://doi.org/10.3892/mco.2022.2594.
Lheureux, S., Braunstein, M., Oza, A.M., 2019a. Epithelial ovarian cancer: evolution of management in the era of precision medicine. CA Cancer J. Clin. 69, 280–304. https://doi.org/10.3322/caac.21559.
Lheureux, S., Gourley, C., Vergote, I., Oza, A.M., 2019b. Epithelial ovarian cancer. Lancet 393, 1240–1253. https://doi.org/10.1016/S0140-6736(18)32552-2.
Liu, J., Song, X., Guo, W., Liu, W., Xu, S., Yang, Y., Chu, X., Lei, Z., 2025. Unlock the code of MHC II-enabled Cancer immunotherapy. Crit. Rev. Oncol. Hematol. 214, 104813. https://doi.org/10.1016/j.critrevonc.2025.104813.
Lohmussaar, K., Boretto, M., Clevers, H., 2020. Human-derived model systems in gynecological cancer research. Trends Cancer 6, 1031–1043. https://doi.org/10.1016/j.trecan.2020.07.007.
Luo, Y., Xia, Y., Liu, D., Li, X., Li, H., Liu, J., Zhou, D., Dong, Y., Li, X., Qian, Y., Xu, C., Tao, K., Li, G., Pan, W., Zhong, Q., Liu, X., Xu, S., Wang, Z., Liu, R., Zhang, W., Shan, W., Fang, T., Wang, S., Peng, Z., Jin, P., Jin, N., Shi, S., Chen, Y., Wang, M., Jiao, X., Luo, M., Gong, W., Wang, Y., Yao, Y., Zhao, Y., Huang, X., Ji, X., He, Z., Zhao, G., Liu, R., Wu, M., Chen, G., Hong, L., Consortium, C., Ma, D., Fang, Y., Liang, H., Gao, Q., 2024. Neoadjuvant PARPi or chemotherapy in ovarian cancer informs targeting effector Treg cells for homologous-recombination-deficient tumors. e4924 Cell 187, 4905–4925. https://doi.org/10.1016/j.cell.2024.06.013.
Macintyre, G., Goranova, T.E., De Silva, D., Ennis, D., Piskorz, A.M., Eldridge, M., Sie, D., Lewsley, L.A., Hanif, A., Wilson, C., Dowson, S., Glasspool, R.M., Lockley, M., Brockbank, E., Montes, A., Walther, A., Sundar, S., Edmondson, R., Hall, G.D., Clamp, A., Gourley, C., Hall, M., Fotopoulou, C., Gabra, H., Paul, J., Supernat, A., Millan, D., Hoyle, A., Bryson, G., Nourse, C., Mincarelli, L., Sanchez, L.N., Ylstra, B., Jimenez-Linan, M., Moore, L., Hofmann, O., Markowetz, F., McNeish, I.A., Brenton, J.D., 2018. Copy number signatures and mutational processes in ovarian carcinoma. Nat. Genet. 50, 1262–1270. https://doi.org/10.1038/s41588-018-0179-8.
McPherson, A., Vazquez-Garcia, I., Myers, M.A., Al-Rawi, D.H., Zatzman, M., Weiner, A. C., Freeman, S., Mohibullah, N., Satas, G., Williams, M.J., Ceglia, N., Norkunaite, D., Zhang, A.W., Li, J., Lim, J.L.P., Wu, M., Choi, S., Havasov, E., Grewal, D., Shi, H., Kim, M., Schwarz, R.F., Kaufmann, T., Dinh, K.N., Uhlitz, F., Tran, J., Wu, Y., Patel, R., Ramakrishnan, S., Kim, D., Clarke, J., Green, H., Ali, E., DiBona, M., Varice, N., Kundra, R., Broach, V., Gardner, G.J., Roche, K.L., Sonoda, Y., Zivanovic, O., Kim, S.H., Grisham, R.N., Liu, Y.L., Viale, A., Rusk, N., Lakhman, Y., Ellenson, L.H., Tavare, S., Aparicio, S., Chi, D.S., Aghajanian, C., Abu-Rustum, N.R., Friedman, C.F., Zamarin, D., Weigelt, B., Bakhoum, S.F., Shah, S.P., 2025. Ongoing genome doubling shapes evolvability and immunity in ovarian cancer. Nature. https://doi.org/10.1038/s41586-025-09240-3.
Nero, C., Vizzielli, G., Lorusso, D., Cesari, E., Daniele, G., Loverro, M., Scambia, G., Sette, C., 2021. Patient-derived organoids and high grade serous ovarian cancer: from disease modeling to personalized medicine. J. Exp. Clin. Cancer Res. 40, 116. https://doi.org/10.1186/s13046-021-01917-7.
Norquist, B.M., Brady, M.F., Harrell, M.I., Walsh, T., Lee, M.K., Gulsuner, S., Bernards, S. S., Casadei, S., Burger, R.A., Tewari, K.S., Backes, F., Mannel, R.S., Glaser, G., Bailey, C., Rubin, S., Soper, J., Lankes, H.A., Ramirez, N.C., King, M.C., Birrer, M.J., Swisher, E.M., 2018. Mutations in homologous recombination genes and outcomes in ovarian carcinoma patients in GOG 218: An NRG oncology/gynecologic oncology group study. Clin. Cancer Res 24, 777–783. https://doi.org/10.1158/1078-0432.CCR-17-1327.
Ovarian Tumor Tissue Analysis, C., Goode, E.L., Block, M.S., Kalli, K.R., Vierkant, R.A., Chen, W., Fogarty, Z.C., Gentry-Maharaj, A., Toloczko, A., Hein, A., Bouligny, A.L., Jensen, A., Osorio, A., Hartkopf, A., Ryan, A., Chudecka-Glaz, A., Magliocco, A.M., Hartmann, A., Jung, A.Y., Gao, B., Hernandez, B.Y., Fridley, B.L., McCauley, B.M., Kennedy, C.J., Wang, C., Karpinskyj, C., de Sousa, C.B., Tiezzi, D.G., Wachter, D.L., Herpel, E., Taran, F.A., Modugno, F., Nelson, G., Lubinski, J., Menkiszak, J., Alsop, J., Lester, J., Garcia-Donas, J., Nation, J., Hung, J., Palacios, J., Rothstein, J. H., Kelley, J.L., de Andrade, J.M., Robles-Diaz, L., Intermaggio, M.P., Widschwendter, M., Beckmann, M.W., Ruebner, M., Jimenez-Linan, M., Singh, N., Oszurek, O., Harnett, P.R., Rambau, P.F., Sinn, P., Wagner, P., Ghatage, P., Sharma, R., Edwards, R.P., Ness, R.B., Orsulic, S., Brucker, S.Y., Johnatty, S.E., Longacre, T.A., Ursula, E., McGuire, V., Sieh, W., Natanzon, Y., Li, Z., Whittemore, A. S., Anna, A., Staebler, A., Karlan, B.Y., Gilks, B., Bowtell, D.D., Hogdall, E., Candido dos Reis, F.J., Steed, H., Campbell, I.G., Gronwald, J., Benitez, J., Koziak, J.M., Chang-Claude, J., Moysich, K.B., Kelemen, L.E., Cook, L.S., Goodman, M.T., Garcia, M.J., Fasching, P.A., Kommoss, S., Deen, S., Kjaer, S.K., Menon, U., Brenton, J.D., Pharoah, P.D.P., Chenevix-Trench, G., Huntsman, D.G., Winham, S.J., Kobel, M., Ramus, S.J., 2017. Dose-response association of CD8+ tumor-infiltrating lymphocytes and survival time in high-grade serous ovarian cancer. JAMA Oncol. 3, e173290. https://doi.org/10.1001/jamaoncol.2017.3290.
Perren, T.J., Swart, A.M., Pfisterer, J., Ledermann, J.A., Pujade-Lauraine, E., Kristensen, G., Carey, M.S., Beale, P., Cervantes, A., Kurzeder, C., du, Bois, A., Sehouli, J., Kimmig, R., Stähle, A., Collinson, F., Essapen, S., Gourley, C., Lortholary, A., Selle, F., Mirza, M.R., Leminen, A., Plante, M., Stark, D., Qian, W.D., Parmar, M.K.B., Oza, A.M., Investigators, I., 2011. A Phase 3 trial of bevacizumab in ovarian cancer. N. Engl. J. Med. 365, 2484–2496. https://doi.org/10.1056/NEJMoa1103799.
Ponton-Almodovar, A., Udumula, M.P., Khullar, V., Rashid, F., Rattan, R., Bernard, J.J., Horibata, S., 2025. GPT2 mediates metabolic alterations in platinum-resistant ovarian cancer cells. Res Sq. https://doi.org/10.21203/rs.3.rs-6480518/v1.

Santoro, A., Angelico, G., Travaglino, A., Inzani, F., Spadola, S., Pettinato, A., Mazzucchelli, M., Bragantini, E., Maccio, L., Zannoni, G.F., 2025. The multiple facets of ovarian high grade serous carcinoma: a review on morphological, immunohistochemical and molecular features. Crit. Rev. Oncol. Hematol. 208, 104603. https://doi.org/10.1016/j.critrevonc.2024.104603.

Shen, Y., Ren, Y., Chen, K., Cen, Y., Zhang, B., Lu, W., Xu, J., 2022. The impact of neoadjuvant chemotherapy on the tumor microenvironment in advanced high-grade serous carcinoma. Oncogenesis 11, 43. https://doi.org/10.1038/s41389-022-00419-1.

Udumula, M.P., Rashid, F., Singh, H., Pardee, T., Luther, S., Bhardwaj, T., Anjaly, K., Piloni, S., Hijaz, M., Gogoi, R., Philip, P.A., Munkarah, A.R., Giri, S., Rattan, R., 2024. Targeting mitochondrial metabolism with CPI-613 in chemoresistant ovarian tumors. J. Ovarian Res. 17, 226. https://doi.org/10.1186/s13048-024-01546-6.

Vanacker, H., Harter, P., Labidi-Galy, S.I., Banerjee, S., Oaknin, A., Lorusso, D., Ray-Coquard, I., 2021. PARP-inhibitors in epithelial ovarian cancer: actual positioning and future expectations. Cancer Treat. Rev. 99, 102255. https://doi.org/10.1016/j.ctrv.2021.102255.

Vaughan, S., Coward, J.I., Bast, R.C., Jr, Berchuck, A., Berek, J.S., Brenton, J.D., Coukos, G., Crum, C.C., Drapkin, R., Etemadmoghadam, D., Friedlander, M., Gabra, H., Kaye, S.B., Lord, C.J., Lengyel, E., Levine, D.A., McNeish, I.A., Menon, U., Mills, G.B., Nephew, K.P., Oza, A.M., Sood, A.K., Stronach, E.A., Walczak, H., Bowtell, D.D., Balkwill, F.R., 2011. Rethinking ovarian cancer: recommendations for improving outcomes. Nat. Rev. Cancer 11, 719–725. https://doi.org/10.1038/nrc3144.

Vazquez-Garcia, I., Uhlitz, F., Ceglia, N., Lim, J.L.P., Wu, M., Mohibullah, N., Niyazov, J., Ruiz, A.E.B., Boehm, K.M., Bojilova, V., Fong, C.J., Funnell, T., Grewal, D., Havasov, E., Leung, S., Pasha, A., Patel, D.M., Pourmaleki, M., Rusk, N., Shi, H., Vanguri, R., Williams, M.J., Zhang, A.W., Broach, V., Chi, D.S., Da Cruz Paula, A., Gardner, G.J., Kim, S.H., Lennon, M., Long Roche, K., Sonoda, Y., Zivanovic, O., Kundra, R., Viale, A., Derakhshan, F.N., Geneslaw, L., Issa Bhaloo, S., Maroldi, A., Nunez, R., Pareja, F., Stylianou, A., Vahdatinia, M., Bykov, Y., Grisham, R.N., Liu, Y. L., Lakhman, Y., Nikolovski, I., Kelly, D., Gao, J., Schietinger, A., Hollmann, T.J., Bakhoum, S.F., Soslow, R.A., Ellenson, L.H., Abu-Rustum, N.R., Aghajanian, C., Friedman, C.F., McPherson, A., Weigelt, B., Zamarin, D., Shah, S.P., 2022. Ovarian cancer mutational processes drive site-specific immune evasion. Nature 612, 778–786. https://doi.org/10.1038/s41586-022-05496-1.

Veneziani, A.C., Gonzalez-Ochoa, E., Alqaisi, H., Madariaga, A., Bhat, G., Rouzbahman, M., Sneha, S., Oza, A.M., 2023. Heterogeneity and treatment landscape of ovarian carcinoma. Nat. Rev. Clin. Oncol. 20, 820–842. https://doi.org/10.1038/s41571-023-00819-1.

Vergote, I., Gonzalez-Martin, A., Lorusso, D., Gourley, C., Mirza, M.R., Kurtz, J.E., Okamoto, A., Moore, K., Kridelka, F., McNeish, I., Reuss, A., Votan, B., du Bois, A., Mahner, S., Ray-Coquard, I., Kohn, E.C., Berek, J.S., Tan, D.S.P., Colombo, N., Zang, R., Concin, N., O'Donnell, D., Rauh-Hain, A., Herrington, C.S., Marth, C., Poveda, A., Fujiwara, K., Stuart, G.C.E., Oza, A.M., Bookman, M.A., participants of the 6th Gynecologic Cancer InterGroup Ovarian Cancer Consensus Conference on Clinical, R, 2022a. Clinical research in ovarian cancer: consensus recommendations from the Gynecologic Cancer InterGroup. Lancet Oncol. 23, e374–e384. https://doi.org/10.1016/S1470-2045(22)00139-5.

Vergote, I., Gonzalez-Martin, A., Ray-Coquard, I., Harter, P., Colombo, N., Pujol, P., Lorusso, D., Mirza, M.R., Brasiuniene, B., Madry, R., Brenton, J.D., Ausems, M., Buttner, R., Lambrechts, D., European experts' consensus, g, 2022b. European experts consensus: BRCA/homologous recombination deficiency testing in first-line ovarian cancer. Ann. Oncol. 33, 276–287. https://doi.org/10.1016/j.annonc.2021.11.013.

Xu, J., Lu, W., Wei, X., Zhang, B., Yang, H., Tu, M., Chen, X., Wu, S., Guo, T., 2024. Single-cell transcriptomics reveals the aggressive landscape of high-grade serous carcinoma and therapeutic targets in tumor microenvironment. Cancer Lett. 593, 216928. https://doi.org/10.1016/j.canlet.2024.216928.

Zhang, K.Y., Erkan, E.P., Jamalzadeh, S., Dai, J., Andersson, N., Kaipio, K., Lamminen, T., Mansuri, N., Huhtinen, K., Carpén, O., Hietanen, S., Oikkonen, J., Hynninen, J., Virtanen, A., Häkkinen, A., Hautaniemi, S., Vähärautio, A., 2022. Longitudinal single-cell RNA-seq analysis reveals stress-promoted chemoresistance in metastatic ovarian cancer. Sci. Adv. 8 https://doi.org/ARTN eabm1831 10.1126/sciadv.abm1831.